Tectonics

RESEARCH ARTICLE
10.1029/2018TC005246

Key Points:
- Magnetotelluric (MT) data in western Zambia show evidence for thin lithosphere beneath an orogenic belt
- The underlying asthenosphere has high conductivity indicative of the presence of melt
- One interpretation is that melt has migrated along the base of the thicker adjacent cratonic lithosphere, thermally eroding the lithosphere beneath the orogenic belt

Supporting Information:
- Supporting Information S1

Correspondence to:
R. L. Evans,
revans@whoi.edu

Citation:
Evans, R. L., Elsenbeck, J., Zhu, J., Abdelsalam, M. G., Sarafian, E., Mutamina, D., et al. (2019). Structure of the lithosphere beneath the Barotse Basin, western Zambia, from magnetotelluric data. *Tectonics*, *38*, 666–686. https://doi.org/10.1029/2018TC005246

Received 18 JUL 2018
Accepted 29 NOV 2018
Accepted article online 30 JAN 2019
Published online 22 FEB 2019

Structure of the Lithosphere Beneath the Barotse Basin, Western Zambia, From Magnetotelluric Data

R. L. Evans[1], J. Elsenbeck[1,2], J. Zhu[1], M. G. Abdelsalam[3], E. Sarafian[4,5], D. Mutamina[6], F. Chilongola[6], E. A. Atekwana[7], and A. G. Jones[8,9]

[1]Department of Geology and Geophysics, Woods Hole Oceanographic Institution, Woods Hole, MA, USA, [2]Now at Lincoln Laboratory, Massachusetts Institute of Technology, Lexington, MA, USA, [3]Boone Pickens School of Geology, Oklahoma State University, Stillwater, OK, USA, [4]WHO/MIT Joint Program in Oceanography, Woods Hole Oceanographic Institution, Woods Hole, MA, USA, [5]Now at Corning Research and Development Corporation, Corning, NY, USA, [6]Geological Survey Department of the Ministry of Mines and Minerals Development for the Government of the Republic of Zambia, Lusaka, Zambia, [7]Department of Geological Sciences, University of Delaware, Newark, DE, USA, [8]Dublin Institute for Advanced Studies, Dublin, Ireland, [9]Now at Complete MT Solutions, Inc., Ottawa, Ontario, Canada

Abstract A magnetotelluric survey in the Barotse Basin of western Zambia shows clear evidence for thinned lithosphere beneath an orogenic belt. The uppermost asthenosphere, at a depth of 60–70 km, is highly conductive, suggestive of the presence of a small amount of partial melt, despite the fact that there is no surface expression of volcanism in the region. Although the data support the presence of thicker cratonic lithosphere to the southeast of the basin, the lithospheric thickness is not well resolved and models show variations ranging from ~80 to 150 km in this region. Similarly variable is the conductivity of the mantle beneath the basin and immediately beneath the cratonic lithosphere to the southeast, although the conductivity is required to be elevated compared to normal lithospheric mantle. In a general sense, two classes of model are compatible with the magnetotelluric data: one with a moderately conductive mantle and one with more elevated conductivities. This latter class would be consistent with the impingement of a stringer of plume-fed melt beneath the cratonic lithosphere, with the melt migrating upslope to thermally erode lithosphere beneath the orogenic belt that is overlain by the Barotse Basin. Such processes are potentially important for intraplate volcanism and also for development or propagation of rifting as lithosphere is thinned and weakened by melt. Both models show clear evidence for thinning of the lithosphere beneath the orogenic belt, consistent with elevated heat flow data in the region.

1. Introduction

The East African Rift System (EARS; e.g., McConnell, 1972), which has formed over the last ~30 Ma, offers a natural laboratory for understanding continental rifting, from the early stages of rift nucleation through transition into seafloor spreading. Due to its prominent surface expression, the rift can be easily followed from the Afar Depression, where a triple junction between the Red Sea, Gulf of Aden, and the Main Ethiopian Rift has been established, through its eastern and western branches that surround the Tanzania craton, to its southern end in the Malawi Rift (Figure 1a). It has long been observed from seismicity that there is a series of rift basins that extend southwestward from the Tanganyika and Malawi rifts to as far as the Okavango rift zone (ORZ) in Botswana, some ~1,700 km away from the Western Branch (Figure 1b; Fairhead & Girdler, 1969; Reeves, 1972; Scholz et al., 1976). This rift system is suggested to represent the southwestern branch (SWB) of the EARS (e.g., Modisi et al., 2000). The SWB appears to be confined to a broad NE trending collage of Paleoproterozoic-Neoproterozoic orogenic belts bounded by the Congo craton in the northwest and the Zimbabwe-Kaapvaal craton to the southeast (Figure 2). We refer to this belt as the Trans-Southern Africa orogenic belt (Figure 2).

The presence of the SWB rift basins, found within the Trans-Southern Africa orogenic belts that border Archean cratons, supports the model of rifting exploiting zones of weakness within thin lithosphere (e.g., Ebinger, 1989; Ebinger & Sleep, 1998; Keranen & Klemperer, 2008; Nyblade & Brazier, 2002). The adjacent thick lithospheric keels offer the possibility of edge-driven convection and subsequent melt generation as a potential mechanism to assist rifting, alternative to the plume-driven rifting thought to occur beneath the Afar Depression (e.g., King & Ritsema, 2000) and also beneath the Tanzania craton (Koptev et al., 2016, 2015).

10.1029/2018TC005246

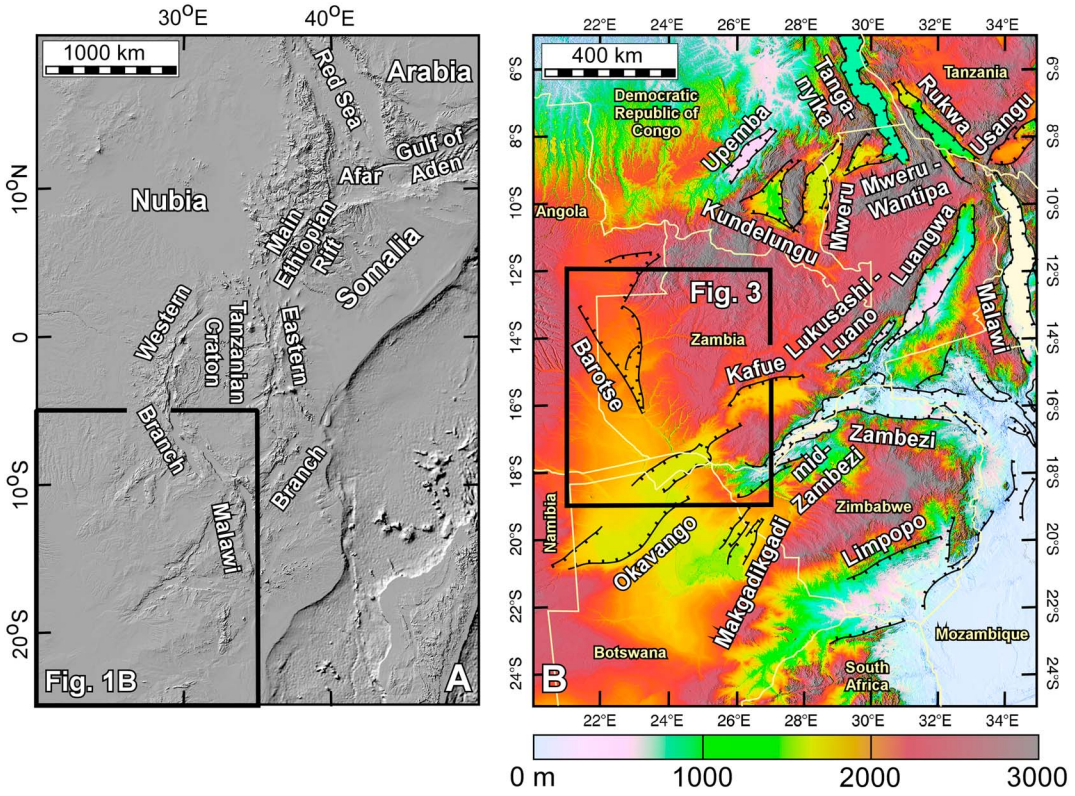

Figure 1. (a) Digital elevation model of the East African Rift System from the most evolved region in the Afar Depression, through the eastern and western branches and toward the southwestern branch. The major plates are the Nubia, Arabia, and Somalia, which join in a triple junction in the Afar Depression. (b) Digital elevation model of the southwestern branch showing its major rift basins.

Significant effort has focused on understanding the evolution of the ORZ as an incipient continental rift representing the youngest segment of the EARS. These efforts include remote sensing, aeromagnetic, shallow magnetotelluric (MT), and electrical resistivity methods (Bufford et al., 2012; Kinabo et al., 2007, 2008). Recently, as part of the PRIDE (Processes of Rift Initiation, Development, and Evolution) project, aeromagnetic and satellite gravity data have been used to examine the thermal and lithospheric structure of the ORZ and the influence of the inherited Precambrian structure in its evolution (Leseane et al., 2015). Additionally, passive seismic studies have been used to further constrain the deeper structure of the ORZ and to suggest possible mechanisms for rift initiation (Yu et al., 2017; Yu, Gao, et al., 2015; Yu, Liu, Moidaki, et al., 2015; Yu, Liu, Reed, et al., 2015).

Little is known about how the ORZ connects to the rest of the EARS. However, on the basis of elevated heat flow, it has long been suggested that the EARS extends through Zambia (Chapman & Pollack, 1975), although the lithospheric structure beneath Zambia remains poorly constrained and there is no obvious surface expression of rifting through this region. The Luangwa rift in eastern Zambia is interpreted as a Paleozoic-Mesozoic (Permian-Triassic; ~300–200 Ma) rift that was developed during the Karoo rifting event during the early stages of fragmentation of Gondwana (e.g., Banks et al., 1995; Daly et al., 1989). It is unclear whether the Luangwa rift is currently active. In southwestern Zambia, there are a number of poorly known ENE and NNW trending extensional structures of late Paleozoic-early Mesozoic (Permian-Jurassic; ~300–145 Ma) age that are possibly Karoo basins that could have been reactivated during the onset of the EARS, hence forming different segments of the SWB. Following Unrug (1987), these are referred to as the Barotse graben, the Kafue graben, and the mid-Zambezi graben (Figure 1b).

Knowledge of the lithospheric structure beneath and surrounding the Barotse Basin in western Zambia (Figure 1b) is critical to understanding the extent of the SWB and its relationship with the underlying Precambrian structure. The MT method has the ability to map variations in lithospheric structure (e.g.,

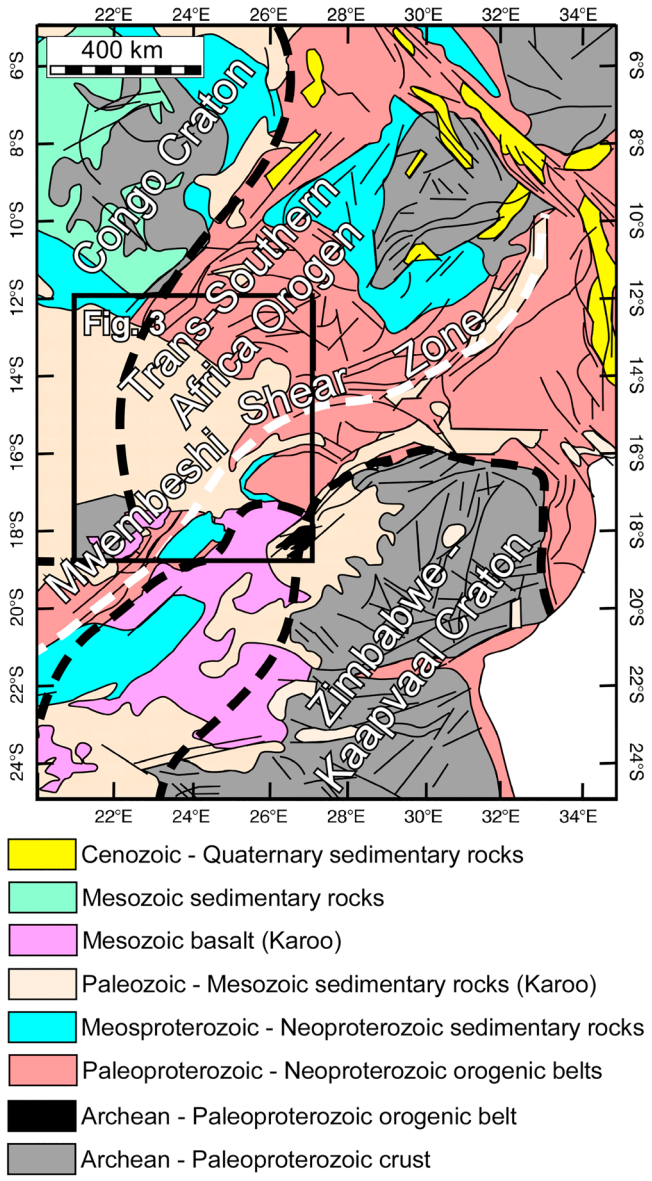

Figure 2. A geologic map showing the relationship of the study area to the primary orogenic belts and cratons in the region. Modified from the International Geological Map of Africa 1:5,000,000 scale. Third edition 1985–1990, Commission of the Geological Map of the World.

Jones et al., 2013) and is thus a useful tool in understanding rifting processes (e.g., Weckmann, 2012). In this paper we report on the results inferred from a MT data set collected in western Zambia as part of the larger PRIDE project studying the incipient stages of continental rifting along the EARS. The data were collected across the Barotse Basin in western Zambia, an area of interest for petroleum exploration. The MT data collected shed light on lithospheric structure through the central portion of the Trans-Southern Africa orogenic belt, the northwestern continuation of the Zimbabwe-Kaapvaal craton, and the transition into the Congo craton in the further northwest (Figure 2).

2. Geological Setting

2.1. Continuation of the EARS Into Zambia?

Although the path of active rifting of the EARS through Zambia remains unclear, the presence of a network of several rift basins suggests possible corridors to form the SWB (e.g., Fairhead & Girdler, 1969; Modisi et al., 2000; Reeves, 1972; Sebagenzi & Kaputo, 2002). This network comprises separate rift basins of different sizes, but they are generally NE trending, extending southwest of the Tanganyika and Malawi rifts (Figure 1b). On the one hand, the rift basins that extend southwest of the Tanganyika rift (Upemba, Kundelungu, Mweru, and Mweru-Wantipa) do not continue a significant distance and are concentrated along the border between Congo and Zambia. On the other hand, the rift basins that extend from the Malawi rift continue southwestward for ~1,700 km along the border between Zambia, Malawi and Mozambique and include the Luangwa, Lukusashi-Luano, Kafue, and mid-Zambezi. These rifts are generally aligned with the NE-SW strike of the ORZ in Botswana. The ORZ is suggested to be as young as 200,000 years (Huntsman-Mapila et al., 2006; Kinabo et al., 2008; Modisi et al., 2000) and less evolved than either the eastern or western branches of the EARS. Very little is known about the structural and tectonic development of different segments of the SWB with the exception of the ORZ, and, to a lesser degree, the Luangwa rift. The rate of extension is unknown, and the absence of magmatism providing surface samples prevents insights into possible lithospheric or asthenospheric processes occurring beneath the rift basins.

The ORZ extends northeastward from northern Botswana into southwestern Zambia (Figure 1b). This rift is characterized by the presence of NE trending border faults (Bufford et al., 2012; Kinabo et al., 2007, 2008) as well as elevated heat flow compared to the surrounding Archean-Paleoproterozoic cratons (Leseane et al., 2015). Strain localization during rift initiation was largely controlled by the presence of the Mesoproterozoic-Neoproterozoic structure associated with the Damara and Ghanzi-Chobe orogenic belts sandwiched between the Congo craton in the northwest and the Magondi belt to the southeast (Figures 2 and 3; Leseane et al., 2015). The Moho is elevated by 4–5 km beneath the rift zone reaching a depth of ~36 km (Yu, Liu, Reed, et al., 2015). Faster NE-SW *S* wave splitting directions are found beneath the ORZ (Yu, Gao, et al., 2015), but no thermal anomalies are seen in the mantle transition zone beneath the rift (Yu, Liu, Moidaki, et al., 2015). Low *P* wave velocity is observed in the upper asthenosphere beneath the rift zone, and this has been interpreted as related to decompressional melting due to lithospheric thinning (Yu et al., 2017). MT data acquired during the Southern Africa Magnetotelluric Experiment (SAMTEX) project (e.g., Jones et al., 2009, 2003–2008; Evans et al., 2011) in northwestern Botswana did not show evidence of lithospheric thinning or reduced resistivities beneath the ORZ that would be associated with the thermal effects that typically accompany rifting (Khoza et al., 2013).

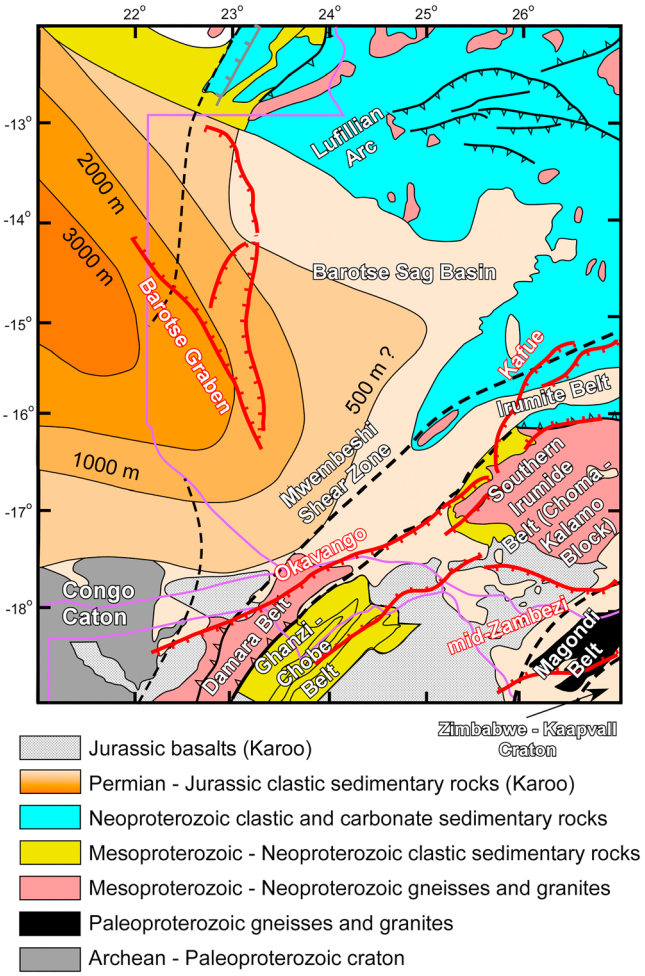

Figure 3. The Barotse Basin and primary tectonic features. Modified from the Tectonic Map of Africa 1:10,000,000 scale, Commission of the Geological Map of the World.

The above geological and geophysical observations indicate that the ORZ represents a juvenile stage of rifting and that it is part of the EARS system. However, this is less clear for other segments of the SWB. The Luangwa rift is considered to have been well developed by the end of the Karoo rifting event that accompanied the early stages of Gondwana fragmentation during late Paleozoic-early Mesozoic (Permian-Triassic; ~300–200 Ma; e.g., Banks et al., 1995; Daly et al., 1989). Nonetheless, the observation that some major faults are sites for hot springs (e.g., Sakungo, 1988) raises the possibility that this rift might be part of the EARS and is currently active. However, Helium isotopic signatures of hot spring fluids do not show a strong mantle component (Wanless et al., 2016). The observation that the Luangwa rift and the underlying Neoproterozoic Mwembeshi "suture" zone are marked by a lithospheric-scale zone of high electrical conductivity (Sarafian et al., 2018) is in agreement with the proposition that the development of the rift was largely controlled by the Precambrian lithospheric heterogeneity (e.g., Banks et al., 1995; Daly et al., 1989).

2.2. The Barotse Basin

There are significant discrepancies in the literature on the way the term "Barotse Basin" is used. Here, we differentiate between the "Barotse intra-continental sag-basin" and the "Barotse graben" (Figure 3). Unrug (1987) used borehole and remote sensing data to suggest that the Barotse Basin is a NNW trending half-graben that extends between northwestern Zambia and eastern Angola (Figure 1b) and that the NNW trending eastern border fault of the half-graben cuts through the Precambrian regional trend possibly exploiting Neoproterozoic Pan-African transcurrent faults. Unrug (1987) considered both the ENE trending Kafue and mid-Zambezi grabens (which hosts exposed basaltic flows) to merge with the eastern side of the Barotse graben. The two ENE trending grabens are separated by the Choma-Kalamo block (Figures 3 and 4; Hanson et al., 1988). Finally, Unrug (1987) suggested that the Kafue graben is influenced by the Mwembeshi dislocation zone (Figure 3) and the mid-Zambezi graben is influenced by the "Zambezi dislocation zone" and that both dislocation zones were developed during the collision of the Congo and the Kalahari (Zimbabwe-Kaapvaal) during the Neoproterozoic Pan-African orogeny.

Here, we regard the Barotse Basin to be the product of three basin formation cycles. The first cycle occurred during the Paleozoic-Mesozoic (Permian-Triassic; ~300–200 Ma) during the early stages of Gondwana fragmentation in the form of broad lithospheric downwarping that was accompanied by local grabens formation such as the Barotse graben. The second cycle took the form of interior sag-basin formation resulting in the deposition of the Mesozoic-Cenozoic sedimentary rocks (Cretaceous to present, 145–0 Ma) of the Kalahari group. The third cycle might have taken the form of graben formation similar to the ORZ and the Makgadikgadi depression (Figure 1b).

2.3. Regional Precambrian Geology

We divide our study area into four Precambrian domains, which are, from northwest to southeast, the Congo craton, the Trans-Southern Africa orogenic belt, and the Zimbabwe-Kaapvaal craton (Figure 2). Synthesis of the Precambrian geology of our study area and surrounding regions can be found in Sarafian et al. (2018) and in Leseane et al. (2015).

2.3.1. The Congo and the Zimbabwe-Kaapvaal Cratons

The Congo craton is a large tract of Archean-Paleoproterozoic continental lithosphere that extends throughout southwestern, western, and central Africa. It is thought to be underlain by a thick cratonic root that reaches ~250 km in its central part (e.g., Abdelsalam et al., 2011). Recently, Yu et al. (2017) observed a

10.1029/2018TC005246

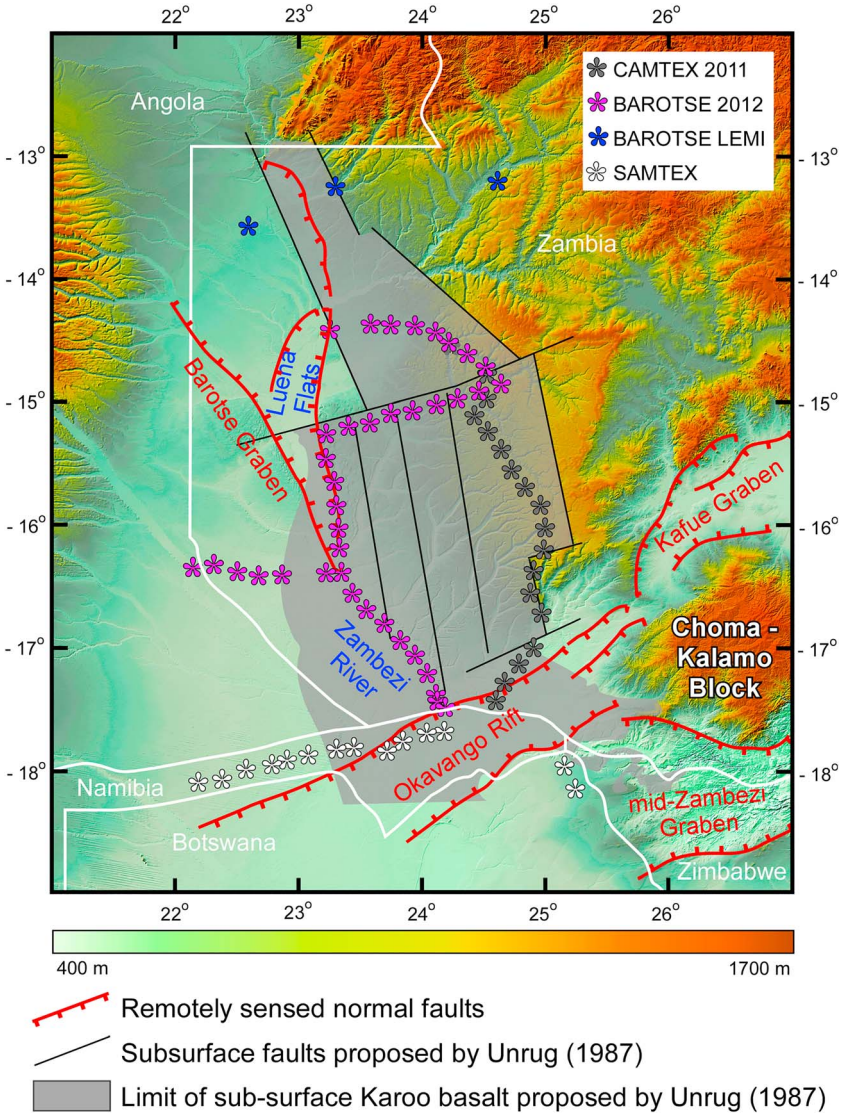

Figure 4. A digital elevation model of the survey area showing the locations of magnetotelluric stations (stars). The magnetotelluric data were collected in several campaigns; brown stars = phase I acquisition; pink stars = phase II acquisition by the Geological Survey Department; blue stars = long-period LEMI stations also collected by the Geological Survey Department; white stars = Southern Africa Magnetotelluric Experiment (SAMTEX) data used for this analysis. Coverage further to the west and north was not possible because of the border with Angola and the difficulty of working in the river valley.

high *P* wave velocity anomaly extending to a depth of ~250–350 km beneath the segment of the Congo craton that is exposed in the southwestern part of our study area (Figure 3). Also, the tectonic map in Figure 3 suggests the presence of a portion of the Congo craton in the northwestern corner of our study area.

The composite Zimbabwe-Kaapvaal craton, also called the Kalahari craton, represents two cratonic blocks that were amalgamated during the late Archean along the Limpopo orogenic belt. It is bounded in the northwest by the Paleoproterozoic Magondi belt (Figures 2 and 3). SAMTEX showed that the lithosphere beneath both the Congo and Zimbabwe-Kaapvaal cratons is thicker than that of the Damara and Ghanzi-Chobe orogenic belts reaching ~180–250 km (Evans et al., 2011; Khoza et al., 2013; Miensopust et al., 2011; Muller et al., 2009).

2.3.2. The Trans-Southern Africa Orogenic Belt

The Trans-Southern Africa orogenic belt in the northeastern part of our study area constitutes, from northwest to southeast, the Neoproterozoic Lufillian arc and the Mesoproterozoic-Neoproterozoic Irumide, and

Southern Irumide orogenic belts (Figures 2 and 3; See summary in Sarafian et al., 2018). In the southwestern part of our study area, and further southwest, this belt comprises, from northwest to southeast, the Neoproterozoic Damara orogenic belt and the Mesoproterozoic Ghanzi-Chobe orogenic belt (Figures 2 and 3; See summary in Leseane et al., 2015).

The Irumide and Southern Irumide orogenic belts (e.g., De Waele et al., 2009; Johnson et al., 2006, 2005) in the northeast can be correlated to the Damara and Ghanzi-Chobe orogenic belts (e.g., Key & Ayres, 2000) to the southeast (Figure 3). Together with the Lufillian arc (e.g., Porada & Berhorst, 2000), these orogenic belt are thought to have formed as a result of collision events between the Congo-Tanzania-Bangweulu craton and the Kalahari craton (Zimbabwe-Kaapvaal). These collisional events followed the formation of oceanic basins during Rodinia fragmentation (e.g., Gray et al., 2008; Hanson, 2003).

The Magondi orogenic belt is exposed on the northwestern margin of the Zimbabwe-Kaapvaal craton, and it is bounded to the northwest by the Choma-Kalamo block (Figure 3; Hanson et al., 1988). Majaule et al. (2001) obtained a U-Pb zircon age of ~2039 Ma from a granitic outcrop within the Magondi belt and interpreted this as the crystallization age. Also, Majaule et al. (2001) obtained U-Pb age of ~2673 Ma from zircon xenocrysts and interpreted this to indicate the presence of an Archean crustal component.

Within the Trans-Southern Africa orogenic belt, between the Choma-Kaloma block and the Irumide belt, exists a band of eclogites, metagabbros, and gabbros with incompatible element patterns indicative of an oceanic origin (John et al., 2003). Although these rocks suggest formation at a mid-ocean ridge, the likely conclusion of the Wilson cycle that formed the orogenic belt was subduction, and the eclogites suggest subduction to a depth of ~90 km around 600 Ma (John et al., 2003).

2.4. Related Regional Geophysical Results

Teleseismic studies have been carried out that focus on the whole of Africa (e.g., Fishwick, 2010) and southern Africa in particular from the Southern Africa Seismic Experiment project (e.g., James et al., 2001; A. Li & Burke, 2006; Y. Yang et al., 2008), and on the active regions of the EARS, particularly with the advent of Africa Array (e.g., Adams & Nyblade, 2011; Hansen et al., 2012; Mulibo & Nyblade, 2013; Nyblade et al., 2008; O'Donnell et al., 2013). However, all of the various models produced have limited resolution in western Zambia. Further north in Zambia, where coverage is greater, there remain significant differences in the models inferred from different seismic analyses or from similar analyses by different authors/groups.

Regional tomographic imaging has been carried out on an extensive African data set that illuminates through the transition zone and shows the relationship between the African superplume and likely melt distributions beneath the EARS (Hansen et al., 2012). At depths of around 400 km there is a large slow velocity anomaly beneath central northern Zambia. Resolution of the model is limited, with amplitudes of anomalies muted beneath the Barotse Basin, although there is a very slight drop in velocities at 150 km, and velocities are certainly not indicative of the cratonic lithosphere, which is clearly seen to the east.

The southwest region of Zambia is generally characterized by relatively low seismic velocities (both shear and compressional) at depths between ~100 and 200 km compared to markedly higher velocities immediately to the northeast (Figure 5; O'Donnell et al., 2013; Mulibo & Nyblade, 2013). The low *P* wave velocities are modeled to extend deeper, to at least the 410-km discontinuity (Mulibo & Nyblade, 2013). Low *P* wave velocities appear to track along the western edge of Zambia at depths greater than 100 km, and an *S* wave velocity model has similar structure (Mulibo & Nyblade, 2013), suggesting that this region marks a possible pathway for the EARS through Zambia (O'Donnell et al., 2013). Velocity anomalies are around −0.7% to −0.8% in *P* wave (approximately half the maximum anomaly observed related to the African superplume) and −0.5% in *S* wave (approximately one quarter the maximum observed anomaly; Mulibo & Nyblade, 2013). Absolute *S* wave velocities are around 4.4–4.5 km/s between ~100- and 140-km depths (O'Donnell et al., 2013). In contrast, surface wave tomography results, developed with three seismic stations in south central Zambia, do not show evidence for anomalous velocities above ~250 km in our study region (Fishwick, 2010). Priestley et al. (2008) argue for high velocities in the upper mantle beneath the Damara orogenic belt although the horizontal resolution of their models is several hundred kilometers, far greater than the width of the belt, calling into question their results.

Extensive electromagnetic profiles have been collected across the adjacent Damara orogenic belt to the southwest of our study region (e.g., De Beer et al., 1975, 1982, 1976; Jones et al., 2009; Khoza et al., 2013;

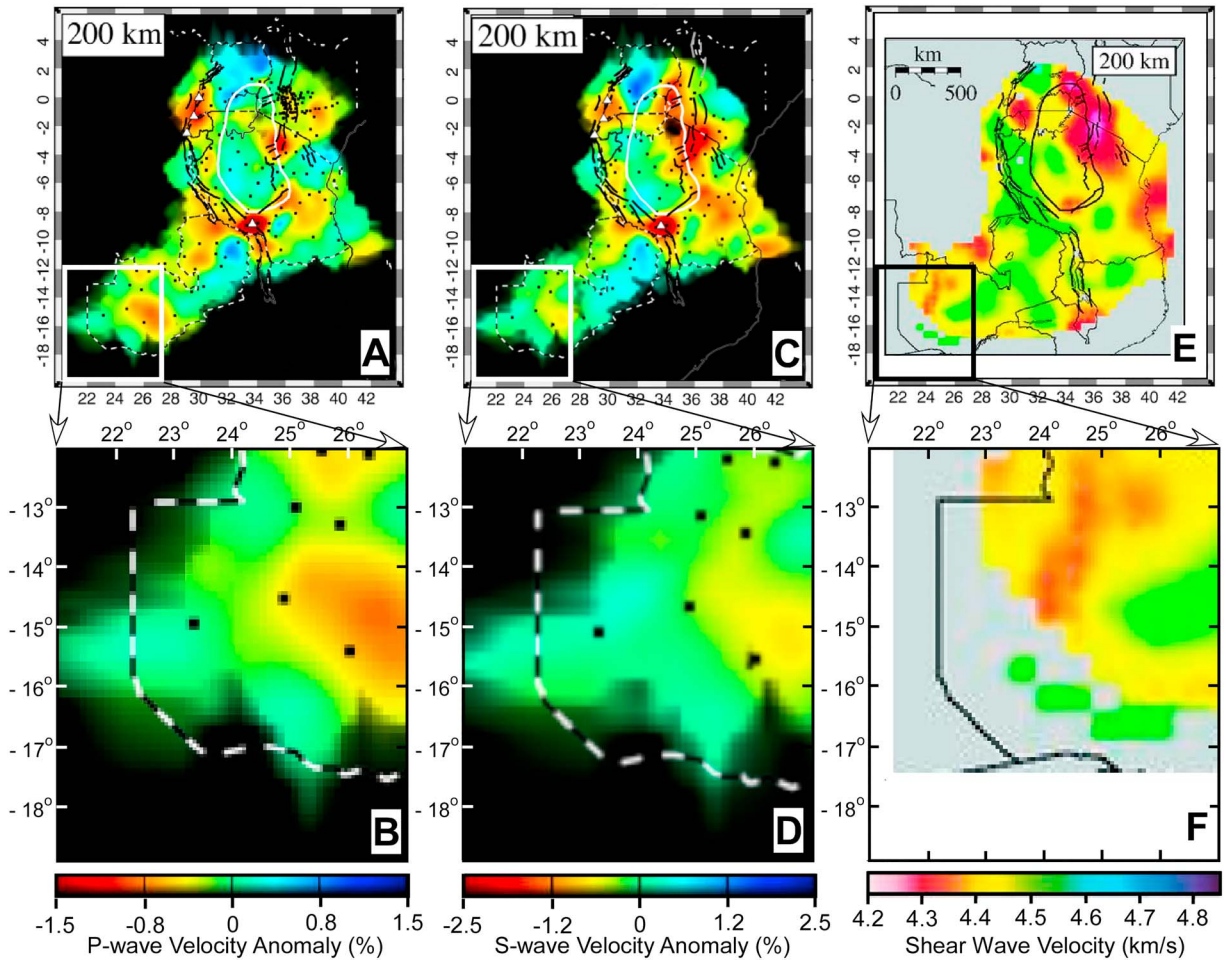

Figure 5. Sections through seismic *P* and *S* wave tomography models from the East African Rift System, including coverage over Zambia. The area of magnetotelluric coverage discussed in this paper is shown by the white rectangles in (a) and (c) and the black rectangle in (e). Models (a)–(d) are from Mulibo and Nyblade (2013) and show a low velocity anomaly centered to the east of our survey area at a depth of 200 km. In contrast, the (e, f) *S* wave model of O'Donnell et al. (2013) shows an anomaly at the northeastern corner of our survey area, although as can be seen from this image, coverage across the Barotse Basin, and hence resolution in our survey area, is limited in this study.

Miensopust et al., 2011; Muller et al., 2009; Ritter et al., 2003; van Zijl, 1978; van Zijl & De Beer, 1983). Within this orogenic belt in northwestern Botswana and northern Namibia, the crust is seen to be electrically conductive and the lithosphere is thinner compared to the abutting cratons (De Beer et al., 1975; Jones et al., 2009; Khoza et al., 2013; Muller et al., 2009; Ritter et al., 2003). The high conductivity of the crust of the orogenic belt is interpreted to be caused by interconnected graphite, sulfides, or other metalliferous minerals deposited along shear zones and related to the known economic deposits of the region. Furthermore, the Lufillian arc section to the northeast of this orogenic belt (Figure 3) defines the well-known and heavily exploited copper-belt region of northern Zambia, suggesting that conductors in the crust could be common in the region. Curiously, the crust and lithosphere beneath the surface mapped location of the Ghanzi-Chobe orogenic belt in northeastern Botswana shows resistive structure with 80-km-thick lithosphere (Miensopust et al., 2011). In contrast, the abutting Magondi orogenic belt to the southeast exhibits high lower crustal conductivity, inferred to be graphite-bearing units correlative over 1,000 km from northeastern Botswana to northwestern Namibia (Miensopust et al., 2011). As an alternative, it has been suggested that increased temperatures associated with rifting or the presence of saline fluids in fractures could explain the high crustal conductivity (De Beer et al., 1975; van Zijl & De Beer, 1983).

Heat flow in Zambia is higher than might be expected given the Precambrian setting, with a mean value of ~67 mW/m^2 (Chapman & Pollack, 1975, 1977; Nyblade et al., 1990; Sebagenzi et al., 1993). This mean value is approximately the same as the value seen at a site in the southeastern corner of our survey area. The high

heat flow suggests some combination of thinned lithosphere (to around 60 km), or an anomalous heat source in the crust or upper mantle (Chapman & Pollack, 1975, 1977; Pollack & Chapman, 1977), and has been used to infer that nascent rifting extends well into Zambia. Indeed, within the Luangwa rift higher heat flow values of ~77 mW/m^2 are seen (Nyblade et al., 1990). Also found in and around the Luangwa rift are hot springs, although there is no obvious mantle signature carried by the waters (Wanless et al., 2016).

3. MT Data Acquisition and Processing

Data were collected at 60 broadband MT stations and three long-period sites located in and around the Barotse Basin (Figure 4). In the resistivity models presented below we have also incorporated data from sites acquired along the Caprivi Strip of northeastern Namibia and in northeastern Botswana as part of the prior SAMTEX campaign (Jones et al., 2009, 2003–2008). For ease of logistics, data were collected along existing roads and tracks. All profiles were collected with approximately 20-km station spacing.

The broadband time series data were recorded using 10 Phoenix Geophysics V5 System 2000's, with each unit containing a data acquisition unit, three Phoenix Geophysics MTC-50 induction coils used to measure the orthogonal horizontal and vertical magnetic field components H_x, H_y, and H_z and five Phoenix Geophysics PE4 Pb-PbCl nonpolarizing electrodes used to measure the orthogonal horizontal electric field components E_x, and E_y with geomagnetic N-S and E-W dipole lengths of approximately 100 m. The time series data were recorded for 2–3 days, resulting in high-quality broadband data at periods of ~0.003 s (384 Hz) to several thousand seconds. The Phoenix instruments record data in separate blocks with different sampling rates and record lengths for short-period and long-period acquisition, with short bursts of high sampling rate acquisition throughout the deployment. This approach permits collection of a wideband data set without requiring a high sampling rate for the full duration of the deployment. The collected time series data were processed using Phoenix Geophysics SSMT2000 processing software, which implements the robust techniques of Jones and Jödicke (1984) and Jones et al. (1989), based on the least trimmed squares method (Rousseeuw, 1984; Rousseeuw & van Driessen, 2006), to estimate MT impedances that were subsequently converted to apparent resistivities and phases. Sites were collected simultaneously allowing the use of remote referencing methods (Gamble et al., 1979) to reduce local biasing.

Subsequent to the main phases of acquisition, three long-period MT sites were acquired by the Geological Survey Department, Zambia, using LEMI-417 units. These instruments were deployed to the northwest of the original survey region and were left in place for ~3 weeks, collecting data at a 1-Hz sampling rate. This longer deployment provides data to periods of around 10,000 s, although the LEMI units do not acquire short-period data, with sensitivity to shallow structure, comparable to the Phoenix MTU devices. Data from the LEMI instruments were processed using the bounded influence code, BIRRP (Chave & Thomson, 2004). Remote reference data used were a combination of an adjacent site and Intermagnet observatory data.

3.1. Modeling

After remote-referenced responses were generated for each station, we assessed the dimensionality of the data and determined the dominant geo-electric strike azimuth. The dominant geo-electric strike azimuths for each line were found using the STRIKE software code (McNeice & Jones, 2001). This code implements a multisite, multifrequency version of the Groom-Bailey decomposition method (Groom & Bailey, 1989) to analyze galvanic distortion and to determine the most consistent geo-electric 2-D strike direction across an MT profile. The dominant strike directions fall between 0°E and 30°E of north. We also carried out a phase tensor analysis (Caldwell et al., 2004) on the data and plot the phase tensor ellipses in map form at four different periods in (supporting information Figure S1). At short periods, large portions of the data are consistent with a 2-D structure, or even a simple 1-D structure for sites within the Barotse Basin itself, reflecting the sedimentary cover. At longer periods, and hence deeper into the Earth, electrical structure becomes more complex. Even allowing for possible 90° ambiguity in strike direction, there are still significant changes in preferred strike direction between sites. Skew values from the phase tensor analysis are highly variable with sites that show high ellipticity generally also showing skew values suggestive of 3-D structure.

As a result of dimensionality analysis we decided that inversions of the data should be performed using two approaches: (1) standard 2-D inversions of subsets of the data, with data fit to a distortion model at a preferred strike direction; and (2) 3-D inversion of the entire data set. There are advantages and

disadvantages to each of these approaches and so we use each in a complementary manner. As the acquisition was, by necessity, along roads, spatial coverage of stations is not ideal for 3-D inversion for which uniform, or close to uniform, spacing is optimal. In contrast, a 2-D inversion makes stringent assumptions about the conductivity distribution with assumed conductivity invariance (transverse electric [TE] mode) parallel to the dominant strike direction. However, 2-D inversions are less computationally expensive, and it is also more common and more routine and straightforward to carry out hypothesis testing on the 2-D inversion results. We have been careful to check for consistency between the 2-D and 3-D results when interpreting models. The 3-D inversion was run first to look for large-scale conductivity features that might dominate the electrical structure and hence control the strike of longer-period data. In addition to orienting 2-D inversion through use of decomposition, we also ran a sequence of inversions with the strike determined by primary features seen in the 3-D inversion. We therefore first describe the 3-D inversion process carried out on the data.

3.2. Three-Dimensional Modeling/Inversion

Three-dimensional inversions of all the data we undertaken with the parallelized Modular Electromagnetic Modeling and Inversion (ModEM) code of Egbert and Kelbert (2012). Additional sites from the prior SAMTEX survey (Jones et al., 2009) were also included to improve spatial coverage to the south. ModEM uses a modular architecture that enables the user to implement a range of model and data space gradient based algorithms. ModEM uses a finite difference, nonlinear conjugate gradient-based algorithm, and regularizes using a model covariance that penalizes deviations from a prior model. We included six MT data components in the inversion: the full impedance tensor (Zxx, Zxy, Zyx, and Zyy) and tipper (Tx and Ty), for 70 stations with data at 32 periods from 0.0018 to ~4,000 s. (The longest period data are recorded on the LEMI instruments in the north of the survey region.) Poor-quality data were removed from the data set, and an error floor of 5% was imposed on impedances and Tipper. The mesh was discretized with cell widths of ~5 km × 5 km in the center of the grid and was composed of a total of 78 cells in the X direction, 111 cells in the Y direction, and 42 cells in the vertical direction. Cell height increases approximately exponentially with depth through the model with the first layer having a thickness of 125 m and the last layer a thickness of 25 km. Meshing was adjusted such that stations are located at the center of cells. We do not include topography in the model. Inversions were initiated with a 100-Ω·m homogeneous half-space starting model. We have run inversions with two different levels of regularization or smoothing parameter (0.3 and 0.5). These two values are not widely varying, and the amounts of structure contained in the resulting models are similar with statistically similar levels of global misfit achieved (1.73 and 1.88), yet each yields final models with subtly different structure, particularly in the eastern part of the model. We have examined misfits of each impedance element and Tipper (supporting information Figures S2 and S3) and find no systematic biases or justification for choosing one model over the other. We have also run an inversion with reduced Tipper error of 2% but with no significant change in model structure. We discuss the implications of these models and the apparent inability of the data to discriminate between them below.

A large conductive feature beneath the Barotse Basin emerged in initial inversions (Figures 6–8), and this was an unexpected and surprising result. In 3-D inversions, the feature first appears in the middle-lower crust, smearing into the upper mantle, at least as far as ~100 km although this is variable through the model (Figures 6 and 7). We have tested whether the feature is purely crustal or whether some elevated conductivity is required in the mantle by removing the feature and restarting the inversion. In this case, an elevated conductivity remains in the mantle, but the anomaly is significantly muted compared to the initial response, suggesting that the high conductivity in the mantle is, to some extent, influenced by regularization. However, the fact that the feature dips and extends to the east leads us to believe that it is not entirely a crustal feature. Further testing of the structure in this part of the mantle has been carried out as part of the 2-D inversion process.

3.3. Two-Dimensional Modeling

The MT responses were imported into Schlumberger's WinGLink software package that employs the regularized, 2-D, finite difference forward and inverse algorithm of Rodi and Mackie (2001). This is an isotropic inversion algorithm that also uses nonlinear conjugate gradient method to minimize model misfit, with control of smoothness set by the regularization parameter tau (τ). The profile the stations included in this inversion are shown in supporting information Figure S4. We ran a series of inversions with a range of τ values

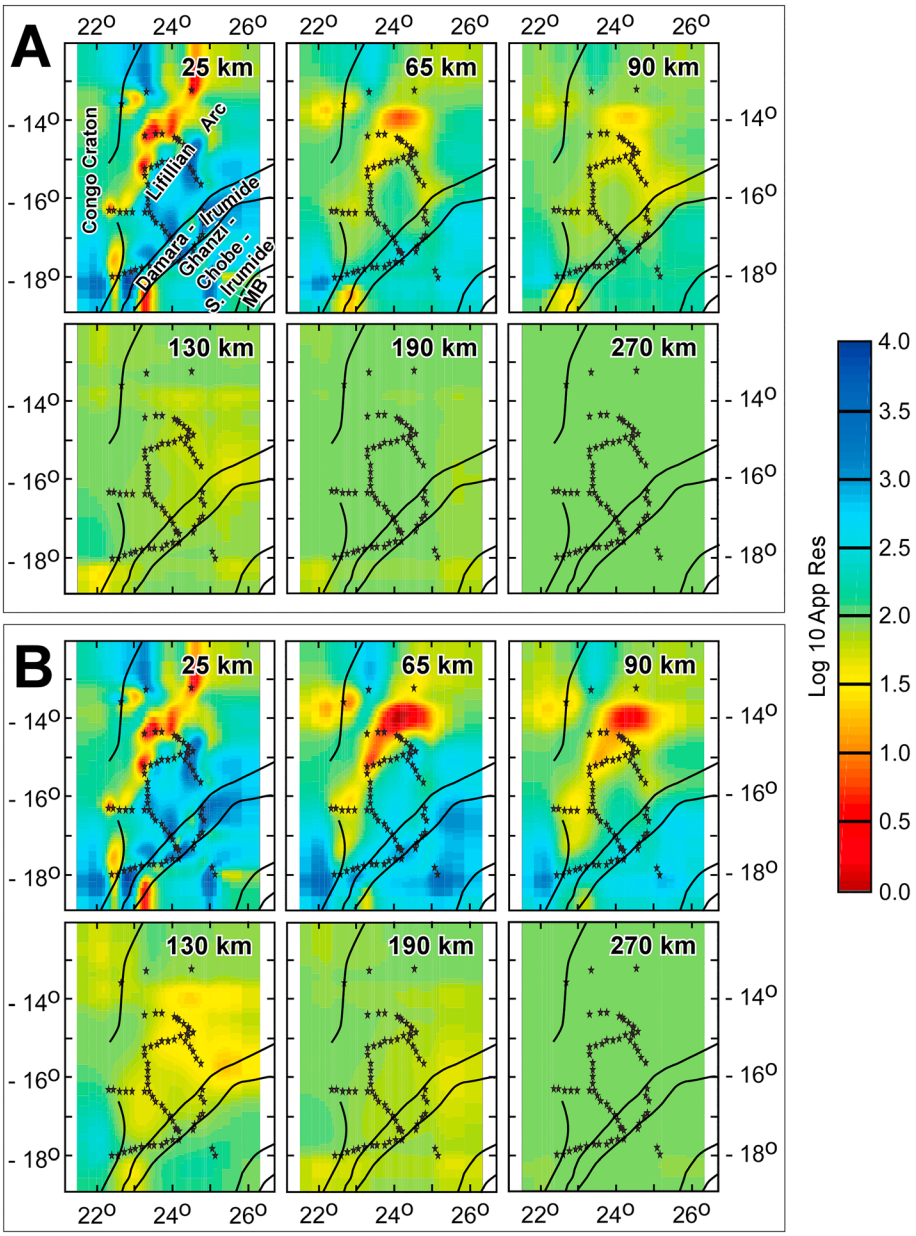

Figure 6. Depth sections of the two acceptable 3-D mantle resistivity models with the depth of each section as labeled. Both axes are distances in hundreds of kilometers. Locations of the magnetotelluric stations used in the inversion are shown by the stars. The difference between the two models are in the regularization parameter with (a) using a value of 0.3 and (b) a value of 0.5.

logarithmically spaced between 0.1 and 100 for each profile to find the models that best minimize misfit without introducing unrealistic or unnecessary structure. We found that τ values between 1 and 3 best met these characteristics. In addition, the algorithm utilizes two additional smoothing parameters (α and β) that can be set to emphasize horizontal structure over vertical features or vice versa. Based on initial tests, we have chosen values of $\alpha = 1.5$ and $\beta = 1.7$ that result in a smooth model with continuous horizontal features. All inversions were initiated with a 100-Ω·m homogeneous half-space starting model and inverted to fit data for both the TE and transverse magnetic modes, with apparent resistivity error floors of 20% and 10%, respectively, and phase error floors of 5% for both modes. The higher error floor was set for the TE mode apparent resistivities as the TE mode data are generally more sensitive to 3-D features (e.g., Jones, 1983; Ledo, 2005; Ledo et al., 2002; Wannamaker et al., 1984). We allowed the

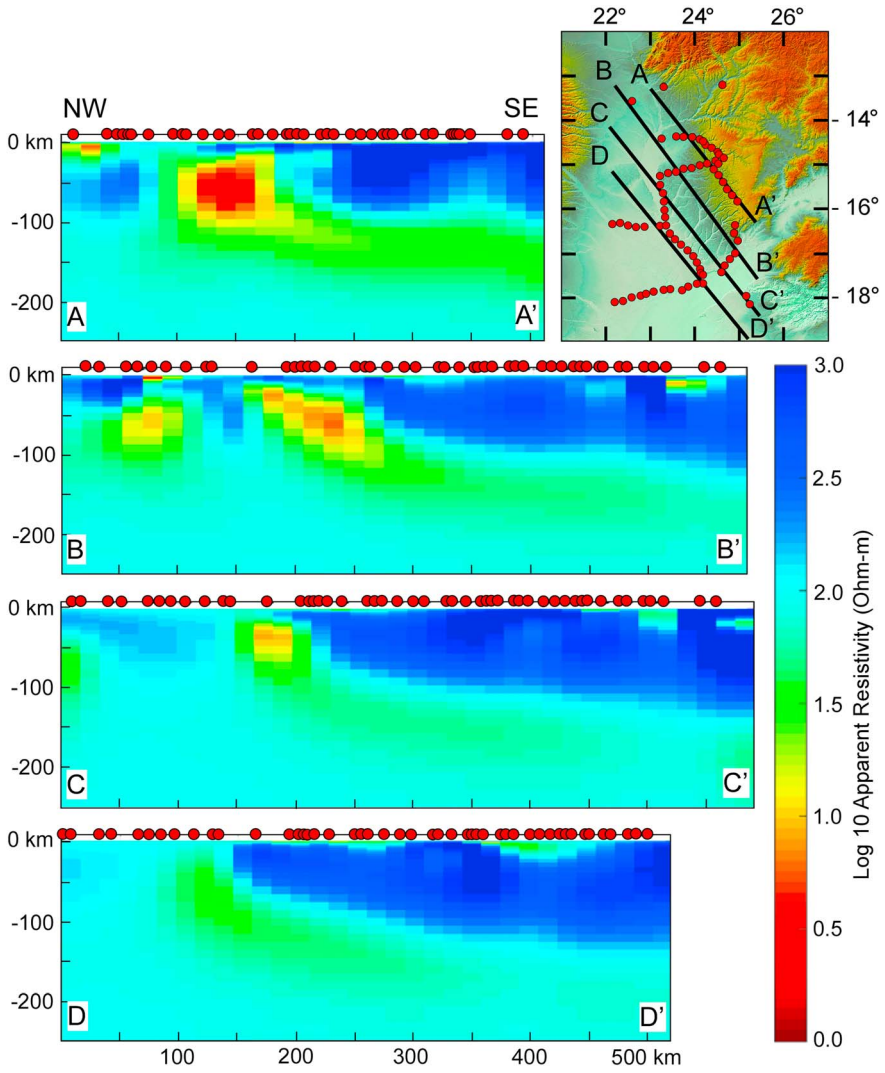

Figure 7. Vertical sections through the model shown in Figure 8b with a smoothing parameter of 0.5. Locations of the sections are as numbered on the inset map.

inversion to solve for static shift effects with no constraints placed on shifts between adjacent sites. The vertical magnetic components, or tipper, are included at all sites where available, with an absolute error floor of 0.05.

Regional galvanic distortions of the study area have been considered by application of the Groom-Bailey decomposition approach (McNeice & Jones, 2001) that used the full period range of the collected data. On examination of the 3-D inversion model, we assumed that the large conductive feature beneath the Barotse Basin would dominate electrical strike. Indeed, the orientation of this feature is consistent with the strike directions determined by decomposition. In this case, we have oriented the profiles used to generate the 2-D model in a direction orthogonal to this feature and project sites onto these profiles accordingly. Data are set in a reference frame such that the TE mode is oriented parallel to the conductor (and hence the direction of invariant conductivity) and the transverse magnetic mode features currents flowing along the profile. As the acquisition geometry was not set up in this orientation, we have run a sequence of inversions using different subsets of the data and inverting them in a similar manner. This approach aims at ensuring consistent features appear in all inversions and that there is no inherent bias in the final model based solely on selection of sites. Additional 2-D inversions were run using decomposed data on profiles with a geometry aligned more closely with that of acquisition and yield results consistent with those presented in Figure 8.

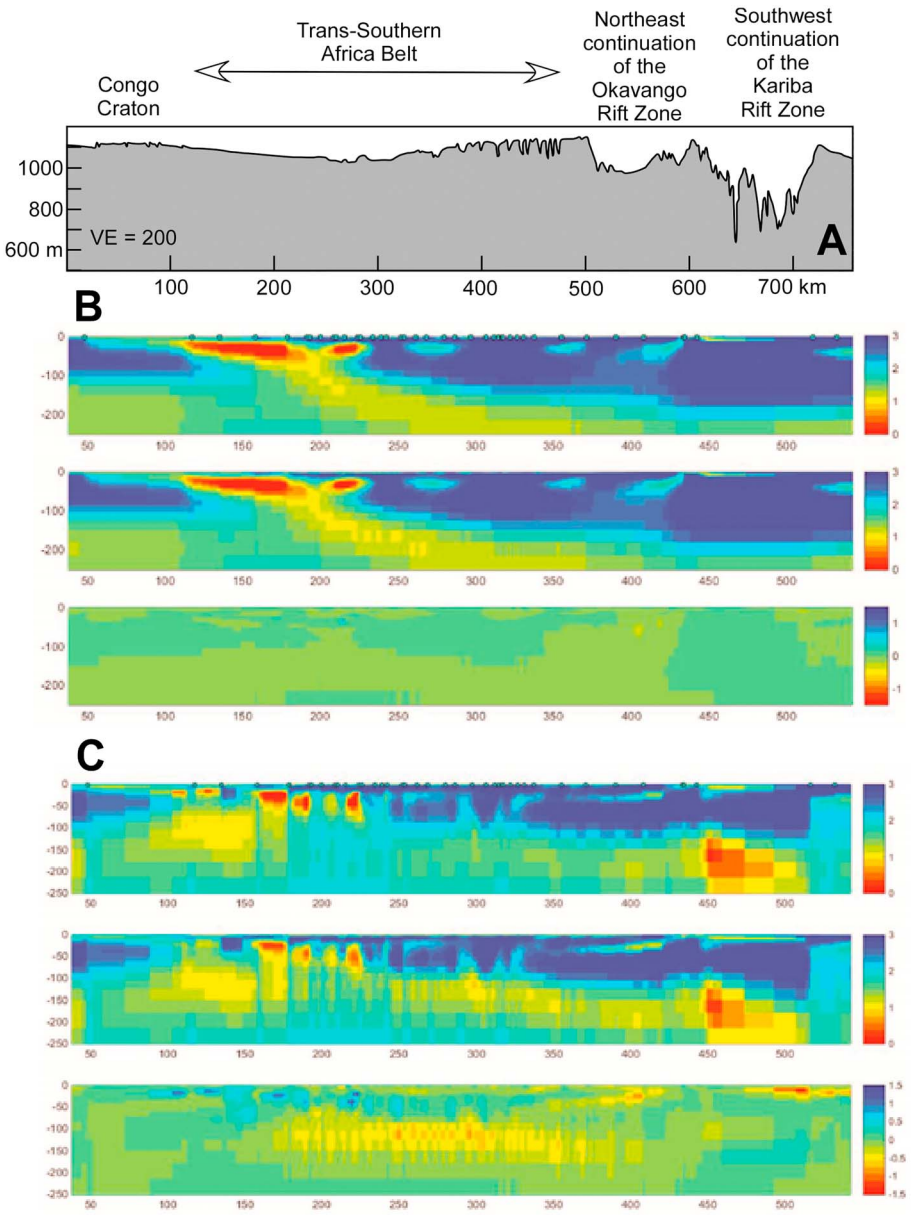

Figure 8. End-member anisotropic 2-D models generated from inverting data from sites across the array projected onto a profile orthogonal to the strike of the conductor seen in 3-D inversions. (a) The location of the profiles with respect to the primary tectonic features traversed. In each sequence of resistivity models (b) and (c), the top figure is the resistivity into the page, the middle shows resistivity parallel to the profile and the bottom panel is the degree of anisotropy between the two models. The root-mean-square misfit of both models is 2.0. Model (b) was obtained using an alpha value of 100, while model (c) uses an alpha value of 1.0. The value of alpha controls the degree of closeness between the resistivities in the along and across strike direction with a smaller value of alpha permitting larger differences or greater anisotropy. In general, both models show a thinning of lithosphere to the west beneath the Barotse Basin and what we infer is Zimbabwe craton lithosphere to the east. However, there is a substantial difference in the thickness of the lithosphere in models (b) and (c), as well as the conductivity of the upper asthenosphere immediately beneath the lithosphere. Station locations projected onto the profile are shown by the circles at the top of the model.

A further set of 2-D models were generated using an anisotropic version of the Rodi and Mackie (2001) inversion code, as described in Baba et al. (2006). Models were started both from a 100-Ω·m half-space and by using the best fit isotropic model from the Winglink inversions as a starting model. The resulting models obtained from these inversions are similar to the isotropic inversions, with the exception that the crustal conductors are anisotropic with higher conductivity, by about an order of magnitude, in the strike direction. We

obtain two classes of models, one with a thicker resistive body (extending to ~180-km depth) to the east and one with a thinner resistor (~120 km), which are equally acceptable in terms of global misfit (2.0) and in terms of fits geographically and to different elements of the impedance tensor. In both cases, the resistor is underlain by conductive mantle, but in the case of the thinner resistive lid, as for the 3-D model, the mantle underneath is appreciably more conductive. End-member models resulting from the anisotropic inversions are shown in Figure 8 and the phase data and response of the more anisotropic of the two models are shown in supporting information Figure S5.

3.4. Sensitivity

The major uncertainties in our modeling results, for both the 2-D and 3-D inversions, are (1) the conductivity of the conductive region of lower crust and upper mantle in the western parts of the survey area and (2) the thickness of the lithosphere to the east and the conductivity of the underlying asthenosphere: The 3-D models generally have thinner lithosphere, but there is variability spatially and between different solutions. The fact that we have several model solutions (Figures 6–8), each of which appears to fit the data satisfactorily, has led us to examine whether there are clues in the particular distributions of misfit that would prefer one solution over the other. We have also carried out a sequence of sensitivity tests for both 2-D and 3-D models, although because of the lighter computational burden, more tests have been carried out on the 2-D models. These tests consist of removing the highly conductive feature from models by replacing high conductivity values with those of the surrounding crust and mantle. Inversions are then restarted and the initial misfit for the perturbed model is compared to the original solution. We also ran the inversion to convergence and examine whether the conductive feature returns and, if it does not, whether there is any significant difference between the misfit of the models with and without conductive features. This kind of test has been used in similar settings before (e.g., Evans et al., 2011; see more details in supporting information). The following two general conclusions can be drawn from the results of these tests:

1. The middle-lower crust beneath the western Barotse Basin is required to be conductive, with resistivity values of around 1–10 Ω·m typical. The high conductivities are concentrated in the northwestern parts of the basin (Figures 6–8).
2. The upper mantle beneath this crustal conductor can have a wide range of acceptable resistivities, from as low as 1 to around 250 Ω·m (see supporting information and Figure S6). For normal smooth inversions, this range is smaller, with values between 1 and ~100 Ω·m at the eastern end of the basin, but with higher values allowable to the west. If a tear is permitted at the base of the crust, then high conductivities are confined to the crust, and the mantle beneath this region can be somewhat more resistive (~250 Ω·m). In all models, the mantle in this ~100-km-wide region is significantly less resistive than the surrounding lithospheric mantle, particularly at the eastern end where there appears to be good evidence for lithospheric thinning or modification over a region ~50 km wide.

Tests on the nature of the lithosphere to the east of the region are inconclusive, and it is clear from the 3-D model that there is variability in thickness through the region that likely makes testing on a 2-D data set difficult. For both 3-D and 2-D models, there is no systematic bias in fits in either a geographical sense or in terms of fits to individual elements of the impedance tensor that allow us to tightly constrain lithospheric thickness. There is a difference in the forward responses of the two 2-D models at long periods primarily in the Tipper, but in both cases, the Tipper is fit to a root-mean-square error of better than 1.0. We conclude that our data simply cannot resolve between the two cases and consider them as end-members in our interpretation and discussion below.

4. Interpretation

4.1. Crustal Structure

Highly conductive lower continental crust is a relatively widespread phenomenon (Jones, 1992), the cause of which has been vigorously debated (see discussion in Evans, 2012, and references therein): The two primary competing interpretations most often advanced are graphite and aqueous fluids, with sulfides playing a role in some settings (see, e.g., the North American Central Plains conductor papers of Jones et al., 1997, and Jones et al., 2005), and partial melt in others (e.g., Wannamaker et al., 2008). There is also often a spatial relationship between crustal conductors and lithospheric suture zones or regional faults (e.g., Evans et al., 2016;

Jones & Garcia, 2006; Murphy & Egbert, 2017; Sarafian et al., 2018). Although graphite and other metalliferous deposits are undoubtedly responsible for upper crustal conductivity anomalies (e.g., ELEKTB Group, 1997), recent work has questioned whether graphite can be stable as an interconnected grain-boundary network under the higher temperatures and pressures found in the lower crust and upper mantle (Yoshino & Noritake, 2011; Zhang & Yoshino, 2017). The high conductivity region seen in the regional model is most prominent in the middle-lower crust. The 2-D anisotropic inversions suggest higher conductivity in the strike direction of the conductor, consistent with fluids in a fabric imparted during formation of the Trans-Southern Africa orogenic belt, or with a solid phase that has been sheared into interconnection along strike, again during formation of the orogenic belt.

4.2. Precambrian Lithospheric Structure

Both the 2-D and 3-D inversion models generated from the data reveal significant lateral variability in lithospheric thickness across western Zambia (Figures 6–8 and supporting information Figure S6). In the southeastern part of our study region, a thicker, more resistive structure is seen (Figures 7 and 8), indicative of cold dry cratonic lithosphere associated with the Zimbabwe craton, although there is significant variation in thickness of the feature between models. The mantle to the northwest of this resistive cratonic region appears to have lower resistivities as discussed in section 3.4 and in the supporting information. Possible explanations for the low resistivities include a combination of high temperatures, hydration of the mantle and partial melting, and the interplay between these mechanisms is discussed in more detail below. The more resistive models suggest a more straightforward structure, most likely a lack of thick lithosphere caused by processes associated with the orogenic belt formation and resulting in an elevated geotherm, consistent with heat flow observations. If temperature is adiabatic (~1450 °C) at 100 km, then resistivities for a dry olivine resistivity would be around 40–50 Ohm·m, consistent with the more moderate solutions for the study region. For the more conductive models, with resistivities of a few ohm-meters, much higher temperatures, well above 1600 °C, would be required, which is clearly not plausible. Thus, more conductive mantle requires a more elaborate explanation. Furthermore, although there are uncertainties in the mantle structure to the southeast, both end-member solutions appear to have a conductive feature that underlies the lithosphere and that appears to connect from deeper in the east to the shallow conductive mantle beneath the Barotse Basin. This feature cannot be thermal and suggests that perhaps other mechanisms are also in play to explain the mantle resistivity beneath the Barotse Basin.

Other mechanisms that can enhance electrical conductivity in the mantle to the levels seen in our most conductive models include the addition of a modest amount of water into olivine and partial melting. Although the two mechanisms are independent, the addition of water lowers the solidus temperature, increasing the likelihood of melting, so there exists a coupling between the two. Although the impact of water on mantle conductivity at high temperatures is controversial (see Evans, 2012, and Naif, 2018, for a discussion), Dai and Karato (2014) suggest that, in the best case scenario, the addition of about 50-ppm water in olivine is able to reduce resistivity to less than 60 Ω·m at temperatures above 1100 °C. Addition of more water to olivine further reduces resistivity, as long as that water can be held by the olivine at the depth of interest. However, a reduction to resistivities of around 1–5 Ω·m requires olivine water contents in excess of 100 ppm at 1400 °C and more than 200 ppm at 1250 °C. These values are the most optimistic case: a model that is an empirical fit to published laboratory data on hydrous olivine conductivity from various groups requires significantly higher olivine water contents to explain even the more modest resistivities seen in our inversion models (Gardes et al., 2014). In this model, resistivity values as low as 5 Ω·m are not predicted for olivine water contents below 200 ppm. However, if resistivities are in the range of 100–200 Ω, uncertainty in temperature, as well as resistivity value, makes predicting water contents difficult. It is important to note that mantle water contents inferred from resistivity values typically refer to the water content in olivine and not the bulk mantle water content. Following the method described in Sarafian et al. (2015), olivine water contents of 50, 100, and 200 ppm correspond to bulk mantle water contents of 215, 430, and 860 ppm, respectively, in the spinel stability field, and the latter two are far too large to be consistent with petrologic estimates of mantle water contents, as we discuss next.

We consider that the mantle beneath the Barotse Basin was at some point in the past associated with a subduction zone setting, as discussed above. Mantle water contents inferred from xenoliths collected in

other paleosubduction settings are consistent with a bulk mantle water content of 100–200 ppm but with typically less than 50 ppm seen in olivine. For example, in the Colorado Plateau, bulk water contents range from 40 to 270 ppm (Z.-X.A. Li et al., 2008). Data from other subduction settings show similar but slightly lower water contents (Peslier et al., 2002; Soustelle et al., 2010), with olivine water contents less than 10 ppm seen in Kamchatka (Soustelle et al., 2010). An explanation for these low water contents in a mantle that has experienced fluxing of fluid from a downgoing wet slab and subsequent melting is beyond the scope of this paper. It is possible that water released from the slab is quickly entrained into the melts generated and so never effectively hydrates the overlying mantle wedge. In any event, the notion that the mantle overlying a subduction zone is extensively hydrated does not appear to be supported by the available xenolith data.

Selway (2015) saw, in effect, the opposite structure to that seen in the Barotse, with highly conductive mantle (a few ohm-meters at depths below ~120 km) beneath the Tanzania craton, with highly resistive structure extending deep beneath the adjacent orogenic belt. This is a puzzling result if explained in terms of mantle hydration as the longevity of cratonic roots is typically explained by a dry composition (Hirth et al., 2000). Selway et al. (2014) explain the high cratonic conductivities by a high water content (~100 ppm in olivine; which is a bulk mantle water content of 430 ppm), although this is assuming the most optimistic conduction enhancement due to the water. Selway (2015) argues that grain size variations are responsible for the difference in strength between the two settings. There are little systematic data on the conductivity effects of grain size, but recent results on the shearing of olivine (Pommier et al., 2018) suggest that smaller grains would be more conductive, the opposite to that seen in the Tanzania craton.

Possibly coupled with elevated water content is the possibility of partial melting. A geotherm consistent with the regional heat flow data and crustal heat production (Chapman & Pollack, 1977) can be constructed that crosses a damp solidus at 50-km depth (0.02 wt% (200 ppm) bulk mantle water content; Katz et al., 2003). Potential upwelling in the mantle resulting from sharp gradients in lithospheric thickness coupled with plate motion (Conrad et al., 2011; Davies & Rawlinson, 2014) could raise the temperatures above this steady state geotherm. Thus, an olivine water content of 50 ppm would bring the mantle very close to the solidus.

Given that the conductivity of the hot, wet matrix comes close to explaining the elevated conductivity, the volumes of melt needed would be modest and would be localized to the high conductive region that dips to the east at the eastern end of the Barotse Basin. Recent work shows that Na concentrations are enhanced at the onset of melting, enhancing melt conductivity (Pommier & Garnero, 2014) and also the addition of a small amount of CO_2 into the melt also results in melt conductivities significantly higher than previously estimated (Sifre et al., 2014). Melt fractions of less than 1% could certainly explain the observed conductivities in the mantle beneath the Barotse Basin, with fractions perhaps as low as 0.2% consistent with observations.

A more tantalizing explanation for the source of melt comes not from the combination of high temperatures and water but from the proximity of the survey region to the African superplume. As discussed above, seismic studies show that the passage of the plume from the deep mantle to upper mantle depths is elongate with primary loci of activity beneath the Afar Depression and also beneath northern Zambia and Malawi (e.g., Hansen et al., 2012). It seems plausible that a stringer of melt related to the plume could impinge on the lithosphere to the east of the Barotse Basin and then migrate along the impermeable base of the lithosphere to the west, rising beneath the Barotse Basin. In this model, the lithosphere could be thin to begin with or have been thermally eroded by the passage over a long duration of small amount of melt. Havlin et al. (2013) have suggested that the passage of small amounts of melt can be sufficient to raise the geotherm without melt expulsion to the surface. In this model, adiabatic temperatures could be reached at ~60-km depth beneath the Barotse Basin, and the combination of this warming and the small melt fraction would be sufficient to explain our resistivities. Melt could percolate upward into the lower crust where it would heat the lower crust, resulting in generation of conductive warm brines (e.g., Wannamaker et al., 2008). It is also possible that the melt freezes, with sulfides carried by the melt responsible for the large crustal conductivities seen.

Other processes have been invoked to explain elevated mantle conductivities in other continental settings. In the failed midcontinent rift in the United States, a similar electrical structure is seen with highly

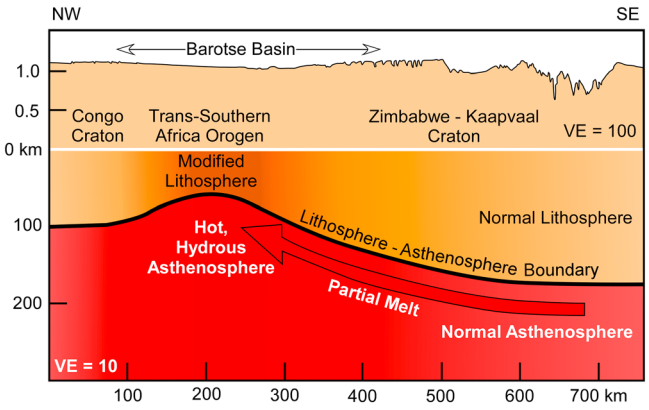

Figure 9. A schematic drawing of the primary tectonic elements and processes inferred from our analysis.

conductive crust indicative of sulfide minerals overlying a moderately conductive mantle (B. Yang et al., 2015). In this case, the authors suggest either graphite or mantle sulfides as an explanation. There are few xenolith data to support abundant graphite in the mantle (Deines, 2002). A suite of xenoliths from the Kaapvaal craton showed graphite in less than 5% of samples, and the graphite observed was disseminated and not in the interconnected network needed to enhance conductivity (Pearson et al., 1994). While sulfides undoubtedly coalesce in the crust to form deposits that impact large-scale conductivity (Jones et al., 1997), the situation in the mantle is less clear. Mantle sulfide concentrations are typically 0.06 wt% (Hart & Gaetani, 2006; Lee et al., 2012) and since sulfide minerals have high density, this corresponds to a smaller percentage by volume. Laboratory measurements of sulfide bearing polycrystalline olivine samples suggests that around 1 vol% sulfide is needed to enhance conductivity (Watson et al., 2010), significantly more than would be expected in the mantle (G. Gaetani, personal communication, September 2015). So, although localized veins of sulfide in the mantle might be possible, it seems unlikely that sulfide would impact such a large extent of mantle as seen in our models.

4.3. Consistency With Seismic Observations

As discussed above, *S* wave velocities are weakly constrained beneath the Barotse Basin. Low velocities (~4.45–4.50 km/s at 70 km) are seen from analyses of surface waves, although the resolution is low due to the lack of surrounding stations. The combined effects of low station density and regularization, both of which tend to damp velocity anomalies, likely mean an uncertainty of up to 0.15 km/s in the shallow mantle (J. P. O'Donnell, personal communication, April 2014). Others have noted a general inability to infer temperatures in the upper mantle to better than about 100 °C from *S* wave velocities (Cammarano et al., 2003), even assuming good constraints on velocity, which is not the case here.

The seismic models of Mulibo and Nyblade (2013; Figure 5) show evidence for a drop in both *P* and *S* wave velocities at 200-km depth to the east of our survey region, although the percentage decreases in velocity are quite modest. In contrast, the tomography model presented by O'Donnell et al. (2013) features a low-velocity anomaly in the northeastern portions of our survey area at the same depth. This discrepancy points to a lack of good coverage in the region and does not help us prefer one resistivity model over the other. However, the recent study by Yu et al. (2017), focused on lithospheric structure beneath the ORZ, also contains a significant low velocity zone at depths below 200 km that extends beneath the Barotse Basin, but once again, this anomaly is at the edge of their coverage area.

5. Conclusions

Based on the range of conductivity models we obtain beneath the Barotse Basin, we suggest the following possible histories for the region:

1. Lithosphere is substantially thinned beneath the Barotse Basin, with the hot underlying asthenosphere containing a small amount of melt. The melt is sourced from the African Superplume and is transported from the base of cratonic lithosphere associated with the Zimbabwe craton, westward and upward along the base of the lithosphere where it pools beneath the region of somewhat thinner lithosphere beneath the Trans-Southern Africa orogenic belt and the overlying Barotse Basin. The migration of the melt might be facilitated by small-scale convection associated with motion of the continent with differential lithospheric thickness across the asthenosphere (e.g., Conrad et al., 2011; Davies & Rawlinson, 2014). A small amount of melt, over time, could thermally erode the lithosphere in the manner suggested by Havlin et al. (2013), raising the geotherm and bulk conductivity beneath the Barotse Basin. The thermal erosion results in elevated mantle temperatures beneath the Barotse Basin but does not result in surface volcanism. A cartoon depicting these processes is shown in Figure 9.
2. The lithosphere beneath the Barotse Basin was extensively modified during the formation of the Trans-Southern Africa orogenic belt and a conductive overprint was imparted onto the mantle. Exactly what this overprint would be is questionable, but it would likely involve a combination of

locally elevated geotherm and the hydration of the asthenospheric mantle, although other explanations are possible.

Whether or not the upper mantle contains melt, the apparent lack of thick lithospheric mantle beneath the Barotse Basin and the underlying Trans-Southern Africa orogenic belt suggests that it would likely represent the focus for continental rifting, allowing melt from depth a more straightforward path to the surface. Rifting in this location would connect the more northerly and mature parts of the EARS with the incipient rifting inferred to be taking place beneath the ORZ. The damp mantle resulting from subduction related amalgamation of the supercontinent Gondwana is inherently primed to both break apart during rifting and to melt, although there is no kinematic signal of rifting in this region, and there is no visible volcanic activity within the crust. Our result appears to support the model of African lithosphere proposed by Ashwal and Burke (1989) in which extensive delamination or loss of lithosphere, and replacement with fertile mantle occurred beneath the orogenic belts during amalgamation of the supercontinent Gondwana.

Acknowledgments
Funding for MT acquisition and analysis was provided by the National Science Foundation grant EAR-1010432 through the Continental Dynamics Program. The data used in this study are available for download at the IRIS Data Management Center through the DOI links cited in Jones et al. (2003–2008; https://doi.org/10.17611/DP/EMTF/SAMTEX) and Evans et al. (2012; https://doi.org/10.17611/DP/EMTF/PRIDE/ZAM). We would like to thank the field crew from the Geological Survey Department, Zambia, for their assistance in collecting data. Matthew Chamberlain, David Margolius, and Colin Skinner, formerly of Northeastern University, are also thanked for their field assistance. Data are available from the corresponding author pending their submission to the IRIS DMC repository at which point they will be publically available. This is Oklahoma State University, Boone Pickens School of Geology contribution number 2019-99.

References

Abdelsalam, M. G., Gao, S. S., & Liégeois, J. P. (2011). Upper mantle structure of the Saharan Metacraton. *Journal of African Earth Sciences*, *60*(5), 328–336. https://doi.org/10.1016/j.jafrearsci.2011.03.009

Adams, A., & Nyblade, A. (2011). Shear wave velocity structure of the southern African upper mantle with implications for the uplift of southern Africa. *Geophysical Journal International*, *186*(2), 808–824. https://doi.org/10.1111/j.1365-246X.2011.05072.x

Ashwal, L. D., & Burke, K. (1989). African lithospheric structure, volcanism and topography. *Earth and Planetary Science Letters*, *96*, 8–14.

Baba, K., Chave, A. D., Evans, R. L., Hirth, G., & Mackie, R. (2006). Mantle dynamics beneath the East Pacific Rise at 17°S: Insights from the Mantle Electromagnetic and Tomography (MELT) experiment. *Journal of Geophysical Research*, *111*, B02101. https://doi.org/10.1029/2004JB003598

Banks, N., Bardwell, K., & Musiwa, S. (1995). Karoo rift basins of the Luangwa Valley, Zambia. *Geological Society, London, Special Publications*, *80*(1), 285–295. https://doi.org/10.1144/GSL.SP.1995.080.01.13

Bufford, K. M., Atekwana, E. A., Abdelsalam, M. G., Shemang, E., Atekwana, E. A., Mickus, K., et al. (2012). Geometry and faults tectonic activity of the Okavango Rift Zone, Botswana: Evidence from magnetotelluric and electrical resistivity tomography imaging. *Journal of African Earth Sciences*, *65*, 61–71. https://doi.org/10.1016/j.jafrearsci.2012.01.004

Caldwell, T. G., Bibby, H. M., & Brown, C. (2004). The magnetotelluric phase tensor. *Geophysical Journal International*, *158*, 457–469.

Cammarano, F., Goes, S., Vacher, P., & Giardini, D. (2003). Inferring upper-mantle temperatures from seismic velocities. *Physics of the Earth and Planetary Interiors*, *138*(3-4), 197–222. https://doi.org/10.1016/S0031-9201(03)00156-0

Chapman, D. S., & Pollack, H. N. (1975). Heat flow and incipient rifting in the central African Plateau. *Nature*, *256*(5512), 28–30. https://doi.org/10.1038/256028a0

Chapman, D. S., & Pollack, H. N. (1977). Heat flow and heat production in Zambia: Evidence for lithospheric thinning in central Africa. *Tectonophysics*, *41*(1-3), 79–100. https://doi.org/10.1016/0040-1951(77)90181-0

Chave, A. D., & Thomson, D. J. (2004). Bounded influence magnetotelluric response function estimation. *Geophysical Journal International*, *157*(3), 988–1006.

Conrad, C. P., Bianco, T. A., Smith, E. I., & Wessel, P. (2011). Patterns of intraplate volcanism controlled by asthenospheric shear. *Nature Geoscience*, *4*(5), 317–321. https://doi.org/10.1038/ngeo1111

Dai, L., & Karato, S.-I. (2014). High and highly anisotropic electrical conductivity of the asthenosphere due to hydrogen diffusion in olivine. *Earth and Planetary Science Letters*, *408*, 79–86. https://doi.org/10.1016/j.epsl.2014.10.003

Daly, M., Chorowicz, J., & Fairhead, J. (1989). Rift basin evolution in Africa: The influence of reactivated steep basement shear zones. *Geological Society, London, Special Publications*, *44*(1), 309–334. https://doi.org/10.1144/GSL.SP.1989.044.01.17

Davies, D. R., & Rawlinson, N. (2014). On the origin of recent intraplate volcanism in Australia. *Geology*, *42*(12), 1031–1034. https://doi.org/10.1130/G36093.1

De Beer, J. H., Gough, D. I., & van Zijl, J. S. V. (1975). An electrical conductivity anomaly and rifting in southern Africa. *Nature*, *255*, 678–680.

De Beer, J. H., Huyssen, R. M. J., Joubert, S. J., & van Zijl, J. S. V. (1982). Magnetometer array studies and deep Schlumberger soundings in the Damara orogenic belt, south West Africa. *Geophysical Journal International*, *70*(1), 11–29. https://doi.org/10.1111/j.1365-246X.1982.tb06388.x

De Beer, J. H., van Zijl, J. S. V., Huyssen, R. M. J., Hugo, P. L. V., Joubert, S. J., & Meyer, R. (1976). A magnetometer array study in south-west Africa, Botswana and Rhodesia. *Geophysical Journal International*, *45*(1), 1–17. https://doi.org/10.1111/j.1365-246X.1976.tb00310.x

De Waele, B., Fitzsimons, I. C. W., Wingate, M. T. D., Tembo, F., Mapani, B., & Belousova, E. A. (2009). The geochronological framework of the Irumide Belt: A prolonged crustal history along the margin of the Bangweulu craton. *American Journal of Science*, *309*(2), 132–187. https://doi.org/10.2475/02.2009.03

Deines, P. (2002). The carbon isotope geochemistry of mantle xenoliths. *Earth Science Reviews*, *58*(3-4), 247–278. https://doi.org/10.1016/S0012-8252(02)00064-8

Ebinger, C. J. (1989). Tectonic development of the western branch of the East African Rift System. *Geological Society of America Bulletin*, *101*(7), 885–903. https://doi.org/10.1130/0016-7606(1989)101<0885:TDOTWB>2.3.CO;2

Ebinger, C. J., & Sleep, N. H. (1998). Cenozoic magmatism throughout East Africa resulting from impact of a single plume. *Nature*, *395*(6704), 788–791. https://doi.org/10.1038/27417

Egbert, G. D., & Kelbert, A. (2012). Computational recipes for electromagnetic inverse problems. *Geophysical Journal International*, *189*(1), 251–267. https://doi.org/10.1111/j.1365-246X.2011.05347.x

ELEKTB Group (1997). KTB and the electrical conductivity of the crust. *Journal of Geophysical Research*, *102*, 18,289–18,305. https://doi.org/10.1029/96JB03861

Evans, R. L. (2012). Chapter 3: Earth's electromagnetic environment. Part 1. Conductivity of Earth materials. In A. D. Chave & A. G. Jones (Eds.), *The magnetotelluric method: Theory and practice* (pp. 50–121). Cambridge, UK: Cambridge University Press.

Evans, R. L., Benoit, M. H., Long, M., Elsenbeck, J., & Ford, H. A. (2016). Evidence for lithospheric loss beneath the Appalachians along the MAGIC line, in AGU Fall Meeting Abstracts.

Evans, R. L., Elsenbeck, J., Mutamina, D., Chilongola, F., Kiyan, D., & Jones, A. G. (2012). Broadband magnetotelluric transfer functions from the Barotse Basin in Zambia. https://doi.org/10.17611/DP/EMTF/PRIDE/ZAM

Evans, R. L., Jones, A. G., Garcia, X., Muller, M., Hamilton, M., Evans, S., et al. (2011). The electrical lithosphere beneath the Kaapvaal Craton, Southern Africa. *Journal of Geophysical Research*, *116*, B04105. https://doi.org/10.1029/2010JB007883

Fairhead, J. D., & Girdler, R. W. (1969). How far does the rift system extend through Africa? *Nature*, *221*(5185), 1018–1020. https://doi.org/10.1038/2211018a0

Fishwick, S. W. (2010). Surface wave tomography: Imaging of the lithosphere-asthenosphere boundary beneath central and southern Africa? *Lithos*, *120*, 63–73. https://doi.org/10.1016/j.lithos.2010.05.011

Gamble, T. D., Goubau, W. M., & Clarke, J. (1979). Magnetotellurics with a remote reference. *Geophysics*, *44*(53–68), 1979.

Gardes, E., Gaillard, F., & Tarits, P. (2014). Toward a unified hydrous olivine electrical conductivity law. *Geochemistry, Geophysics, Geosystems*, *15*, 4984–5000. https://doi.org/10.1002/2014GC005496

Gray, D. R., Foster, D. A., Meert, J. G., Goscombe, B. D., Armstrong, R., Trouw, R. A. J., & Passchier, C. W. (2008). A Damara orogen perspective on the assembly of southwestern Gondwana. *Geological Society of London, Special Publication*, *294*(1), 257–278. https://doi.org/10.1144/SP294.14

Groom, R. W., & Bailey, R. C. (1989). Decomposition of magnetotelluric impedance tensors in the presence of local three-dimensional galvanic distortion. *Journal of Geophysical Research*, *94*, 1913–1925. https://doi.org/10.1029/JB094iB02p01913

Hansen, S., Nyblade, A. A., & Benoit, M. H. (2012). Mantle structure beneath Africa and Arabia from adaptively parameterized P-wave tomography: Implications for the origin of Cenozoic Afro-Arabian tectonism. *Earth and Planetary Science Letters*, *319-320*, 23–34. https://doi.org/10.1016/j.epsl.2011.12.023

Hanson, R. E. (2003). Proterozoic geochronology and tectonic evolution of southern Africa. In M. Yoshida, B. F. Windley, & S. Dasgupta (Eds.), *Proterozoic East Gondwana: Supercontinent assembly and breakupSpecial Publication* (Vol. 206, pp. 427–463). London: Geological Society of London. https://doi.org/10.1144/GSL.SP.2003.206.01.20

Hanson, R. E., Wilson, T. J., Brueckner, H. K., Onstott, T. C., Wardlaw, M. S., Johns, C. C., & Hardcastle, K. C. (1988). Reconnaissance geochronology, tectonothermal evolution and regional significance of the middle Proterozoic Choma-Kalomo Block, southern Zambia. *Precambrian Research*, *42*(1-2), 39–61. https://doi.org/10.1016/0301-9268(88)90009-5

Hart, S. R., & Gaetani, G. (2006). Mantle Pb paradoxes: The sulfide solution. *Contributions to Mineralogy and Petrology*, *152*(3), 295–308. https://doi.org/10.1007/s00410-006-0108-1

Havlin, C., Parmentier, E. M., & Hirth, G. (2013). Dike propagation driven by melt accumulation at the lithosphere–asthenosphere boundary. *Earth and Planetary Science Letters*, *376*, 20–28. https://doi.org/10.1016/j.epsl.2013.06.010

Hirth, G., Evans, R. L., & Chave, A. D. (2000). Comparison of continental and oceanic mantle electrical conductivity: Is the Archean lithosphere dry? *Geochemistry, Geophysics, Geosystems*, *1*(12), 1030. https://doi.org/10.1029/2000GC000048

Huntsman-Mapila, P., Ringrose, S., Mackay, A. W., Downey, W. S., Modisi, M., Coetzee, S. H., et al. (2006). Use of the geochemical and biological sedimentary record in establishing palaeo-environments and climate change in the Lake Ngami basin, NW Botswana. *Quaternary International*, *148*(1), 51–64. https://doi.org/10.1016/j.quaint.2005.11.029

James, D. E., Fouch, M. J., VanDecar, J. C., & van der Lee, S. (2001). Tectospheric structure beneath southern Africa. *Geophysical Research Letters*, *28*(13), 2485–2488. https://doi.org/10.1029/2000GL012578

John, T., Schenk, V., Haase, K., Scherer, E., & Tembo, F. (2003). Evidence for a Neoproterozoic ocean in south-central Africa from mid-oceanic-ridge–type geochemical signatures and pressure-temperature estimates of Zambian eclogites. *Geology*, *31*(3), 243–246. https://doi.org/10.1130/0091-7613(2003)031<0243:EFANOI>2.0.CO;2

Johnson, S., De Waele, B., & Liyungu, K. (2006). U-Pb sensitive high-resolution ion microprobe (SHRIMP) zircon geochronology of granitoid rocks in eastern Zambia: Terrane subdivision of the Mesoproterozoic Southern Irumide Belt. *Tectonics*, *25*, TC6004. https://doi.org/10.1029/2006TC001977

Johnson, S. P., Rivers, T., & De Waele, B. (2005). A review of the Mesoproterozoic to early Paleozoic magmatic and tectonothermal history of south-central Africa: Implications for Rodinia and Gondwana. *Journal of the Geological Society of London*, *162*(3), 433–450. https://doi.org/10.1144/0016-764904-028

Jones, A. G. (1983). The problem of current channelling: A critical review. *Surveys in Geophysics*, *6*(79–122), 1983.

Jones, A. G. (1992). Electrical conductivity of the continental lower crust. *Continental Lower Crust*, 81–143.

Jones, A. G., Chave, A. D., Auld, D., Bahr, K., & Egbert, G. (1989). A comparison of techniques for magnetotelluric response function estimation. *Journal of Geophysical Research*, *94*(14), 201–14,213. https://doi.org/10.1029/JB094iB10p14201

Jones, A. G., Evans, R. L., Muller, M., Hamilton, M., Miensopust, M. P., Garcia, X., et al. (2009). Area selection for diamonds using magnetotellurics: Examples from southern Africa. *Lithos*, *112*(1), 83–92.

Jones, A. G., Evans, R. L., Muller, M. R., Hamilton, M. P., Miensopust, M. P., Garcia, X., et al. (2003–2008). Southern Africa magnetotelluric transfer functions. https://doi.org/10.17611/DP/EMTF/SAMTEX

Jones, A. G., Fishwick, S., Evans, R. L., Muller, M. M., & Fullea, J. (2013). Velocity-conductivity relations for cratonic lithosphere and their application: Example of southern Africa. *Geochemistry, Geophysics, Geosystems*, *14*, 806–827. https://doi.org/10.1002/ggge.20075

Jones, A. G., & Garcia, X. (2006). Electrical resistivity structure of the Yellowknife River Fault Zone and surrounding region. Gold in the Yellowknife Greenstone Belt, Northwest Territories: Results of the EXTECH III Multidisciplinary Research Project, published by Geological Association of Canada, Mineral Deposits Division, Special Publication No. 3, Chapter 10, 126–141, 2006.

Jones, A. G., & Jödicke, H. (1984). Magnetotelluric transfer function estimation improvement by a coherence-based rejection technique. Contributed paper at: 54th SEG, Atlanta, Georgia, 2–6 December, 3, 51–55.

Jones, A. G., Katsube, T. J., & Schwann, P. (1997). The longest conductivity anomaly in the world explained: Sulphides in fold hinges causing very high electrical anisotropy. *Journal of Geomagnetism and Geoelectricity*, *49*(11), 1619–1629. https://doi.org/10.5636/jgg.49.1619

Jones, A. G., Ledo, J., & Ferguson, I. J. (2005). Electromagnetic images of the Trans-Hudson orogen: The North American Central Plains anomaly revealed. *Canadian Journal of Earth Sciences*, *42*(4), 457–478. https://doi.org/10.1139/E05-018

Katz, R. F., Spiegelman, M., & Langmuir, C. H. (2003). A new parameterization of hydrous melting. *Geochemistry, Geophysics, Geosystems*, *4*(9), 1073. https://doi.org/10.1029/2002GC000433

Keranen, K., & Klemperer, S. L. (2008). Discontinuous and diachronous evolution of the Main Ethiopian Rift: Implications for development of continental rifts. *Earth and Planetary Science Letters*, *265*(1-2), 96–111. https://doi.org/10.1016/j.epsl.2007.09.038

Key, R. M., & Ayres, N. (2000). The 1998 edition of the national geological map of Botswana. *Journal of African Earth Sciences*, *30*(3), 427–451.

Khoza, D., Jones, A. G., Muller, M., Evans, R. L., Miensopust, M., & Webb, S. (2013). Lithospheric structure of an Archean craton and adjacent mobile belt revealed from 2D and 3D inversion of magnetotelluric data: Example from southern Congo craton in northern Namibia. *Journal of Geophysical Research: Solid Earth*, *118*, 4378–4397. https://doi.org/10.1002/jgrb.50258

Kinabo, B. D., Atekwana, E. A., Hogan, J. P., Modisi, M. P., & Kampunzu, A. B. (2007). Early structural development of the Okavango rift zone, NW Botswana. *Journal of African Earth Sciences*, *48*(2-3), 125–136. https://doi.org/10.1016/j.jafrearsci.2007.02.005

Kinabo, B. D., Hogan, J. P., Atekwana, E. A., Abdelsalam, M. G., & Modisi, M. P. (2008). Fault growth and propagation during incipient continental rifting: Insights from a combined aeromagnetic and Shuttle Radar Topography mission digital elevation model investigation of the Okavango Rift Zone, northwest Botswana. *Tectonics*, *27*, TC3013. https://doi.org/10.1029/2007TC002154

King, S. D., & Ritsema, J. (2000). African hot spot volcanism: Small-scale convection in the upper mantle beneath cratons. *Science*, *290*(5494), 1137–1140. https://doi.org/10.1126/science.290.5494.1137

Koptev, A., Burov, E., Calais, E., Leroy, S., Gerya, T., Guillou-Frottier, L., & Cloetingh, S. (2016). Contrasted continental rifting via plume-craton interaction: Applications to central East African Rift. *Geoscience Frontiers*, *7*(2), 221–236. https://doi.org/10.1016/j.gsf.2015.11.002

Koptev, A., Calais, E., Burov, E., Leroy, S., & Gerya, T. (2015). Dual continental rift systems generated by plume-lithosphere interaction. *Nature Geoscience*, *8*(5), 388–392. https://doi.org/10.1038/NGEO2401

Ledo, J. (2005). 2-D versus 3-D magnetotelluric data interpretation. *Surveys in Geophysics*, *26*(5), 511–543. https://doi.org/10.1007/s10712-005-1757-8

Ledo, J., Queralt, P., Marti, A., & Jones, A. G. (2002). Two-dimensional interpretation of three-dimensional magnetotelluric data: An example of limitations and resolution. *Geophysical Journal International*, *150*(1), 127–139. https://doi.org/10.1046/j.1365-246X.2002.01705.x

Lee, C.-T. A., Luffi, P., Chin, E. J., Bouchet, R., Dasgupta, R., Morton, D. M., Le Roux, V., et al. (2012). Copper systematics in arc magmas and implications for crust-mantle differentiation. *Science*, *336*(6077), 64–68. https://doi.org/10.1126/science.1217313

Leseane, K., Atekwana, E. A., Mickus, K. L., Abdelsalam, M. G., Shemang, E. M., & Atekwana, E. A. (2015). Thermal perturbations beneath the incipient Okavango Rift Zone, northwest Botswana. *Journal of Geophysical Research: Solid Earth*, *120*, 1210–1228. https://doi.org/10.1002/2014JB011029

Li, A., & Burke, K. (2006). Upper mantle structure of southern Africa from Rayleigh wave tomography. *Journal of Geophysical Research*, *111*, B10303. https://doi.org/10.1029/2006JB004321

Li, Z.-X. A., Lee, C. T., Peslier, A. H., Lenardic, A., & Mackwell, S. J. (2008). Water contents in mantle xenoliths from the Colorado Plateau and vicinity: Implications for the mantle rheology and hydration-induced thinning of continental lithosphere. *Journal of Geophysical Research*, *113*, B09210. https://doi.org/10.1029/2007JB005540

Majaule, T., Hanson, R. E., Key, R. M., Singletary, S. J., Martin, M. W., & Bowring, S. A. (2001). The Magondi Belt in Northeast Botswana: Regional relations and new geochronological data from the Sua Pan area. *Journal of African Earth Sciences*, *32*(2), 257–267. https://doi.org/10.1016/S0899-5362(01)90006-5

McConnell, R. (1972). Geological development of the rift system of eastern. *Africa: Geological Society of America Bulletin*, *83*(9), 2549–2572.

McNeice, G. W., & Jones, A. G. (2001). Multisite, multi-frequency tensor decomposition of magnetotelluric data. *Geophysics*, *66*(1), 158–173. https://doi.org/10.1190/1.1444891

Miensopust, M. P., Jones, A. G., Muller, M. R., Garcia, X., & Evans, R. L. (2011). Lithospheric structures and geometries in northeastern Botswana revealed through SAMTEX magnetotelluric profiling. *Journal of Geophysical Research*, *116*, B02401. https://doi.org/10.1029/2010JB007740

Modisi, M. P., Atekwana, E. A., & Kampunzu, A. B. (2000). Rift kinematics during the incipient stages of continental extension: Evidence from nascent Okavango rift basin, northwest Botswana. *Geology*, *28*(10), 939–942. https://doi.org/10.1130/0091-7613(2000)28<939:RKDTIS>2.0.CO;2

Mulibo, G. D., & Nyblade, A. A. (2013). The *P* and *S* wave velocity structure of the mantle beneath eastern Africa and the African superplume anomaly. *Geochemistry, Geophysics, Geosystems*, *14*, 2696–2715. https://doi.org/10.1002/ggge.20150

Muller, M. R., Jones, A. G., Evans, R. L., Grütter, H. S., Hatton, C., Garcia, X., Hamilton, M. P., et al., & The SAMTEX Team (2009). Lithospheric structure, evolution and diamond prospectivity of the Rehoboth Terrane and western Kaapvaal Craton, southern Africa: Constraints from broadband magnetotellurics. *Lithos*, *112*(1), 93–105.

Murphy, B. S., & Egbert, G. D. (2017). Electrical conductivity structure of southeastern North America: Implications for lithospheric architecture and Appalachian topographic rejuvenation. *Earth and Planetary Science Letters*, *462*, 66–75. https://doi.org/10.1016/j.epsl.2017.01.009

Naif, S. (2018). An upper-bound on the conductivity of hydrated oceanic mantle at the onset of dehydration melting. *Earth and Planetary Science Letters*, *482*, 357–366. https://doi.org/10.1016/j.epsl.2017.11.024

Nyblade, A., Dirks, P., Durrheim, R., Webb, S., Jones, M., Cooper, G., & Graham, G. (2008). Africa array: Developing a geosciences workforce for Africa's natural resource sector. *The Leading Edge*, *27*(10), 1358–1361. https://doi.org/10.1190/1.2996547

Nyblade, A. A., & Brazier, R. A. (2002). Precambrian lithospheric controls on the development of the East African Rift System. *Geology*, *30*(8), 755–758. https://doi.org/10.1130/0091-7613(2002)030<0755:PLCOTD>2.0.CO;2

Nyblade, A. A., Pollack, H. N., Jones, D. L., Podmore, F., & Mushayandebyu, M. (1990). Terrestrial heat flow in east and southern Africa. *Journal of Geophysical Research*, *95*(B11), 17,371–17,384. https://doi.org/10.1029/JB095iB11p17371

O'Donnell, J. P., Adams, A., Nyblade, A. A., Mulibo, G. D., & Tugume, F. (2013). The uppermost mantle shear wave velocity structure of eastern Africa from Rayleigh wave tomography: Constraints on rift evolution. *Geophysical Journal International*, *194*(2), 961–978. https://doi.org/10.1093/gji/ggt135

Pearson, D. G., Boyd, F. R., Haggerty, S. E., Pasteris, J. D., Field, S. W., Nixon, P. H., & Pokhilenko, N. P. (1994). The characterization and, origin of graphite in cratonic lithospheric mantle: A petrological carbon isotope and Raman spectroscopic study. *Contributions to Mineralogy and Petrology*, *115*(4), 449–466. https://doi.org/10.1007/BF00320978

Peslier, A. H., Luhr, J. F., & Post, J. (2002). Low water contents in pyroxenes from spinel-periodotites of the oxidized, sub-arc matle wedge. *Earth and Planetary Science Letters*, *201*(1), 69–86. https://doi.org/10.1016/S0012-821X(02)00663-5

Pollack, H. N., & Chapman, D. S. (1977). On the regional variation of heat flow, geotherms, and lithospheric thickness. *Tectonophysics*, *38*(3-4), 279–296. https://doi.org/10.1016/0040-1951(77)90215-3

Pommier, A., & Garnero, E. J. (2014). Petrology-based modeling of mantle melt electrical conductivity and joint interpretation of electromagnetic and seismic results. *Journal of Geophysical Research: Solid Earth*, *119*, 4001–4016. https://doi.org/10.1002/2013JB010449

Pommier, A., Kohlstedt, D. L., Hansen, L. N., Mackwell, S., Tasaka, M., Heidelbach, F., & Leinenweber, K. (2018). Transport properties of olivine grain boundaries from electrical conductivity experiments. *Contributions to Mineralogy and Petrology*, *173*, 1–13.

Porada, H., & Berhorst, V. (2000). Towards a new understanding of the Neoproterozoic-Early Palaeozoic Lufilian and northern Zambezi Belts in Zambia and the Democratic Republic of Congo. *Journal of African Earth Sciences*, *30*(3), 727–771. https://doi.org/10.1016/S0899-5362(00)00049-X

Priestley, K., McKenzie, D., Debayle, E., & Pilidou, S. (2008). The African upper mantle and its relationship to tectonics and surface geology. *Geophysical Journal International*, *175*(3), 1108–1126. https://doi.org/10.1111/j.1365-246X.2008.03951.x

Reeves, C. V. (1972). Rifting in the Kalahari? *Nature*, *237*(5350), 95–96. https://doi.org/10.1038/237095a0

Ritter, O., Weckmann, U., Vietor, T., & Haak, V. (2003). A magnetotelluric study of the Damara Belt in Namibia 1. Regional scale conductivity anomalies. *Physics of the Earth and Planetary Interiors*, *138*(2), 71–90. https://doi.org/10.1016/S0031-9201(03)00078-5

Rodi, W., & Mackie, R. L. (2001). Nonlinear conjugate gradients algorithm for 2-D magnetotelluric inversion. *Geophysics*, *66*(1), 174–187. https://doi.org/10.1190/1.1444893

Rousseeuw, P. J. (1984). Least median of squares regression. *Journal of the American Statistical Association*, *79*(388), 871–880. https://doi.org/10.1080/01621459.1984.10477105

Rousseeuw, P. J., & van Driessen, K. (2006). Computing LTS regression for large data sets, data min. *Knowledge Discovery*, *12*(1), 29–45. https://doi.org/10.1007/s10618-005-0024-4

Sakungo, F. K. (1988). Geothermal resources of Zambia. *Geothermics*, *17*(2–3), 503–514. https://doi.org/10.1016/0375-6505(88)90079-X

Sarafian, E., Evans, R. L., Abdelsalam, M. G., Atekwana, E., Elsenbeck, J., Jones, A. G., & Chikambwe, E. (2018). Imaging Precambrian lithospheric structure in Zambia using electromagnetic methods. *Gondwana Research*, *54*, 38–49. https://doi.org/10.1016/j.gr.2017.09.007

Sarafian, E., Evans, R. L., Collins, J., Elsenbeck, J., Gaetani, G., Gaherty, J., Hirth, G., et al. (2015). The electrical structure of the central Pacific upper mantle constrained by the NoMelt experiment. *Geochemistry, Geophysics, Geosystems*, *16*, 1115–1132. https://doi.org/10.1002/2014GC005709

Scholz, C. H., Koczynski, T. A., & Hutchins, D. G. (1976). Evidence for incipient rifting in southern Africa. *Geophysical Journal International*, *44*(1), 135–144. https://doi.org/10.1111/j.1365-246X.1976.tb00278.x

Sebagenzi, M. N., & Kaputo, K. (2002). Geophysical evidences of continental break up in the southeast of the Democratic Republic of Congo and Zambia (Central Africa). In S. A. P. L. Cloetingh & Z. Ben-Avraham (Eds.), *From continental extension to collision: Africa-Europe interaction, the Dead Sea and analogue natural laboratories Stephan Mueller Special Publication Series* (Vol. 2, pp. 193–206). EGU European Geosciences Union.

Sebagenzi, M. N., Vasseur, G., & Louis, P. (1993). First heat flow determinations from southeastern Zaire (Central Africa). *Journal of African Earth Sciences*, *16*(4), 413–423. https://doi.org/10.1016/0899-5362(93)90100-5

Selway, K. (2015). Negligible effect of hydrogen content on plate strength in East Africa. *Nature Geoscience*, *8*(7), 543–546. https://doi.org/10.1038/ngeo2453

Selway, K., Yi, J., & Karato, S. I. (2014). Water content of the Tanzanian lithosphere from magnetotelluric data: Implications for cratonic growth and stability. *Earth and Planetary Science Letters*, *388*, 175–186. https://doi.org/10.1016/j.epsl.2013.11.024

Sifre, D., Gardes, E., Massuyeau, M., Hashim, L., Hier-Majumder, S., & Gaillard, F. (2014). Electrical conductivity during incipient melting in the oceanic low-velocity zone. *Nature*, *509*(7498), 81–85. https://doi.org/10.1038/nature13245

Soustelle, V., Tommasi, A., Demouchy, S., & Ionov, D. A. (2010). Deformation and fluid-rock interaction in the supra-subduction mantle: Microstructures and water contents in peridotite xenoliths from the Avacha volcano, Kamchatka. *Journal of Petrology*, *51*(1-2), 363–394. https://doi.org/10.1093/petrology/egp085

Unrug, R. (1987). Tectonic position of Karoo basalts, western Zambia. In *Gondwana six: Structure, tectonics and geophysicsGeophysical Monograph Series* (Vol. 40, pp. 319–322). Washington, DC: American Geophysical Union.

Wanless, V. D., Kurz, M. D., Elsenbeck, J., Curtice, J., Shaw, A. M., & Atekwana, E. A. (2016). Helium isotopes in hot spring gases as magmatic tracers during incipient rifting in Malawi and Zambia, AGU Fall Meeting Abstracts.

Wannamaker, P. E., Hasterok, D. P., Johnston, J. M., Stodt, J. A., Hall, D. B., Sodergren, T. L., et al. (2008). Lithospheric dismemberment and magmatic processes of the Great Basin–Colorado Plateau transition, Utah, implied from magnetotellurics. *Geochemistry, Geophysics, Geosystems*, *9*, Q05019. https://doi.org/10.1029/2007GC001886

Wannamaker, P. E., Hohmann, G. W., & Ward, S. H. (1984). Magnetotelluric responses of 3-dimensional bodies in layered Earths. *Geophysics*, *49*(9), 1517–1533. https://doi.org/10.1190/1.1441777

Watson, H. C., Roberts, J. J., & Tyburczy, J. A. (2010). Effect of conductive impurities on electrical conductivity in polycrystalline olivine. *Geophysical Research Letters*, *37*, L02302. https://doi.org/10.1029/2009GL041566

Weckmann, U. (2012). Making and breaking of a continent: Following the scent of geodynamic imprints on the African continent using magnetotellurics. *Surveys in Geophysics*, *33*(1), 107–134. https://doi.org/10.1007/s10712-011-9147-x

Yang, B., Egbert, G. D., Kelbert, A., & Meqbel, N. M. (2015). Three-dimensional electrical resistivity of the north-central USA from EarthScope long period magnetotelluric data. *Earth and Planetary Science Letters*, *422*, 87–93.

Yang, Y., Li, A., & Ritzwoller, M. H. (2008). Crustal and uppermost mantle structure in southern Africa revealed from ambient noise and teleseismic tomography. *Geophysical Journal International*, *174*(1), 235–248. https://doi.org/10.1111/j.1365-246X.2008.03779.x

Yoshino, T., & Noritake, F. (2011). Unstable graphite films on grain boundaries in crustal rocks. *Earth and Planetary Science Letters*, *306*, 186–192. https://doi.org/10.1016/j.epsl.2011.04.003

Yu, Y., Gao, S. S., Moidaki, M., Reed, C. A., & Liu, K. H. (2015). Seismic anisotropy beneath the incipient Okavango rift: Implications for rifting initiation. *Earth and Planetary Science Letters*, *430*, 1–8. https://doi.org/10.1016/j.epsl.2015.08.009

Yu, Y., Liu, K. H., Huang, Z., Zhao, D., Reed, C. A., Moidaki, M., Lei, J., et al. (2017). Mantle structure beneath the incipient Okavango rift zone in southern Africa. *Geosphere*, *13*(1), 102–111. https://doi.org/10.1130/GES01331.1

Yu, Y., Liu, K. H., Moidaki, M., Reed, C. A., & Gao, S. S. (2015). No thermal anomalies in the mantle transition zone beneath an incipient continental rift: evidence from the first receiver function study across the Okavango Rift Zone, Botswana. *Geophysical Journal International*, *202*, 1407–1418.

Yu, Y., Liu, K. H., Reed, C. A., Moidaki, M., Mickus, K., Atekwana, E. A., & Gao, S. S. (2015). A joint receiver function and gravity study of crustal structure beneath the incipient Okavango Rift, Botswana. *Geophysical Research Letters*, *42*, 8398–8405. https://doi.org/10.1002/2015GL065811

Zhang, B., & Yoshino, T. (2017). Effect of graphite on the electrical conductivity of the lithospheric mantle. *Geochemistry, Geophysics, Geosystems*, *18*, 23–40. https://doi.org/10.1002/2016GC006530

van Zijl, J. S. V. (1978). The relationship between the deep electrical resistivity structure and tectonic provinces in southern Africa-Part 1. Results obtained by Schlumberger soundings. *South African Journal of Geology*, *81*(2), 129–142.

van Zijl, J. S. V., & De Beer, J. H. (1983). Electrical structure of the Damara orogen and its tectonic significance. In *Evolution of the Damara Orogen of South West Africa/Namibia. National Geodynamics ProgrammeSpecial Publication* (Vol. 11, pp. 369–379). Johannesburg: Geological Society of South Africa.